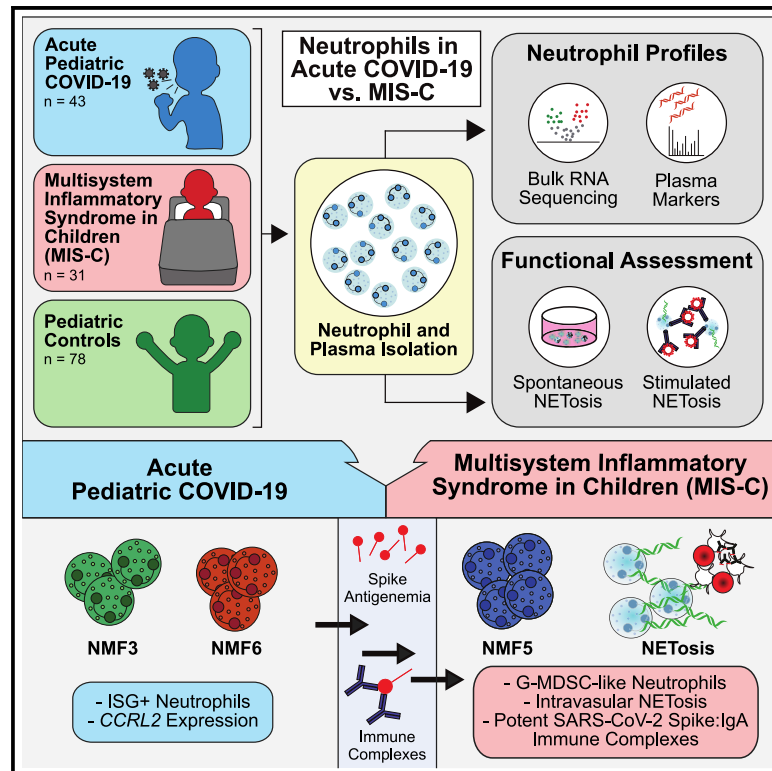Article

Neutrophil profiles of pediatric COVID-19 and multisystem inflammatory syndrome in children

Graphical abstract

Authors

Brittany P. Boribong, Thomas J. LaSalle,
Yannic C. Bartsch, ..., Daniel Irimia,
Moshe Sade-Feldman, Lael M. Yonker

Correspondence

msade-feldman@mgh.harvard.edu (M.S.-F.),
lyonker@mgh.harvard.edu (L.M.Y.)

In brief

Boribong, LaSalle, et al. extensively profile gene expression, protein production, and functionality of neutrophils from children with acute COVID-19 or multisystem inflammatory syndrome in children (MIS-C) to define neutrophil responses driving distinct SARS-CoV-2 disease states. They propose a model whereby neutrophil activation elicits endothelial dysfunction and cardiovascular complications within MIS-C.

Highlights

- Neutrophils in pediatric COVID-19 express an interferon-stimulated gene response

- MIS-C neutrophils display a granulocytic myeloid-derived suppressor cell signature

- Neutrophil activation and extensive spontaneous NETosis are seen in MIS-C

- SARS-CoV-2 spike immune complexes, especially IgA immune complexes, trigger NETs

CellPress

Article

Neutrophil profiles of pediatric COVID-19 and multisystem inflammatory syndrome in children

Brittany P. Boribong,[1,2,3,13] Thomas J. LaSalle,[4,5,6,13] Yannic C. Bartsch,[3,7] Felix Ellett,[8] Maggie E. Loiselle,[1] Jameson P. Davis,[1] Anna L.K. Gonye,[4,5] David B. Sykes,[9,10] Soroush Hajizadeh,[3,4,5] Johannes Kreuzer,[3,4] Shiv Pillai,[3,7] Wilhelm Haas,[3,4] Andrea G. Edlow,[3,11,12] Alessio Fasano,[1,2,3] Galit Alter,[3,7] Daniel Irimia,[8] Moshe Sade-Feldman,[3,4,5,*] and Lael M. Yonker[1,2,3,14,*]

[1]Mucosal Immunology and Biology Research Center, Massachusetts General Hospital, Boston, MA 02114, USA
[2]Department of Pediatrics, Massachusetts General Hospital, Boston, MA 02114, USA
[3]Harvard Medical School, Boston, MA 02115, USA
[4]Center for Cancer Research, Department of Medicine, Massachusetts General Hospital, Boston, MA 02114, USA
[5]Broad Institute of MIT and Harvard, Cambridge, MA 02142, USA
[6]Program in Health Sciences and Technology, Harvard Medical School & Massachusetts Institute of Technology, Boston, MA 02115, USA
[7]Ragon Institute of MGH, MIT, and Harvard, Cambridge, MA 02139, USA
[8]Center for Engineering in Medicine and Surgery, Department of Surgery, Massachusetts General Hospital, Shriners Burns Hospital, Harvard Medical School, Boston, MA 02114, USA
[9]Center for Regenerative Medicine, Massachusetts General Hospital, Boston, MA 02114, USA
[10]Harvard Stem Cell Institute, Cambridge, MA 02138, USA
[11]Department of Obstetrics and Gynecology, Division of Maternal-Fetal Medicine, Boston, MA 02114, USA
[12]Vincent Center for Reproductive Biology, Massachusetts General Hospital, Boston, MA 02114, USA
[13]These authors contributed equally
[14]Lead contact
*Correspondence: msade-feldman@mgh.harvard.edu (M.S.-F.), lyonker@mgh.harvard.edu (L.M.Y.)
https://doi.org/10.1016/j.xcrm.2022.100848

SUMMARY

Multisystem inflammatory syndrome in children (MIS-C) is a delayed-onset, COVID-19-related hyperinflammatory illness characterized by severe acute respiratory syndrome coronavirus 2 (SARS-CoV-2) antigenemia, cytokine storm, and immune dysregulation. In severe COVID-19, neutrophil activation is central to hyperinflammatory complications, yet the role of neutrophils in MIS-C is undefined. Here, we collect blood from 152 children: 31 cases of MIS-C, 43 cases of acute pediatric COVID-19, and 78 pediatric controls. We find that MIS-C neutrophils display a granulocytic myeloid-derived suppressor cell (G-MDSC) signature with highly altered metabolism that is distinct from the neutrophil interferon-stimulated gene (ISG) response we observe in pediatric COVID-19. Moreover, we observe extensive spontaneous neutrophil extracellular trap (NET) formation in MIS-C, and we identify neutrophil activation and degranulation signatures. Mechanistically, we determine that SARS-CoV-2 immune complexes are sufficient to trigger NETosis. Our findings suggest that hyperinflammatory presentation during MIS-C could be mechanistically linked to persistent SARS-CoV-2 antigenemia, driven by uncontrolled neutrophil activation and NET release in the vasculature.

INTRODUCTION

Neutrophil activation is a central component of the immune response against severe acute respiratory syndrome coronavirus 2 (SARS-CoV-2) infection; however, excessive neutrophil hyperactivation can contribute to severe COVID-19 in adults.[1–4] The role of neutrophils in pediatric SARS-CoV-2 infections has not been defined. Children are less likely to suffer serious symptoms of acute COVID-19, but some children can develop a severe, life-threatening hyperinflammatory illness called multisystem inflammatory syndrome in children (MIS-C) weeks to months after the resolution of upper respiratory tract symptoms.[5] MIS-C is defined by sepsis-like physiology with high fevers, systemic inflammation, and multiorgan involvement,

likely caused by SARS-CoV-2 antigenemia originating from gastrointestinal sources of virus leaking across a permeable mucosal barrier into circulation.[6] Children with MIS-C display signs of vascular injury, including elevated C-reactive protein, erythrocyte sedimentation rate, and D-dimer. 80% of children with MIS-C develop cardiac complications, including myocarditis, ventricular dysfunction, and coronary aneurysms,[7,8] although mechanisms of cardiovascular injury are unclear.

Neutrophils play a significant role in innate immune responses against bacterial, fungal, and viral infections.[9] However, at the same time, hyperactivation of neutrophils has been shown to be detrimental in severe diseases, including sepsis, acute respiratory distress syndrome (ARDS), and severe acute COVID-19 in adults.[1,8,10,11] Not only can hyperactivation of polymorphonuclear

Table 1. Patient demographics and distribution of pediatric blood samples used for each assay

Total enrolled (n = 152)	Pediatric controls (n = 78)	COVID-19 (n = 43)	MIS-C (n = 31)
Age, mean years (min, max)	10.9 (1.2, 20)	14.2 (0.04, 22.2)	7.4 (0.17, 21)
Female gender, n (%)	39 (50)	14 (33)	9 (29)
Male gender, n (%)	39 (50)	29 (67)	22 (71)
Race, n (%)			
White	43 (55)	15 (34)	13 (42)
Black or African American	3 (4)	4 (9)	5 (16)
Asian	7 (9)	2 (5)	2 (6)
Ethnicity, n (%)			
Hispanic or Latino	28 (36)	21 (51)	13 (42)
Samples used in assays, n			
RNA sequencing	12	19	17
Proteomics	23	19	13
Cell-free DNA	21	23	19
Spontaneous NETosis	14	0	7

See also Tables S1 and S2.

leukocytes (PMNs) result in vascular and organ injury, but they can also contribute to hypercoagulation and thrombus formation.[12] Understanding neutrophil activation in acute pediatric COVID-19 and MIS-C is essential to developing clinical guidelines and advances in treatment recommendations.

Extensive immune profiling has shown distinct hyperinflammatory patterns distinguishing acute pediatric COVID-19 from MIS-C;[13–15] however, very little information on neutrophil activation has been included in these reports. This paucity of research on neutrophil activation in acute pediatric COVID-19 and MIS-C may be due to technical challenges with studying neutrophils: neutrophils have a very short lifespan and are extensively damaged by freezing. In contrast to peripheral blood mononuclear cells (PBMCs), neutrophils require isolation and fixation or analysis within hours of blood collection. Thus, a significant knowledge gap exists between pediatric COVID-19 and MIS-C and the contribution of neutrophils to disease pathogenesis.

Here, we isolated neutrophils immediately after blood collection from children with acute COVID-19 and MIS-C and healthy controls. We also extensively profiled gene expression, protein production, and neutrophil functionality to define neutrophil responses driving these distinct SARS-CoV-2 disease states in children.

RESULTS

Cohort characteristics

Blood was collected from 152 children, including 43 children with COVID-19 confirmed by RT-PCR (Table S1), 31 children clinically diagnosed with MIS-C (Table S2), and 78 pediatric controls, including healthy children, children with convalescent COVID-19, and children with non-COVID-19 illness. The average ages of the acute pediatric COVID-19 cohort, the MIS-C cohort, and the pediatric control cohort were 14.2, 7.4, and 10.9 years, respectively. Gender, race, and ethnicity are shown in Table 1. Immediately after blood collection, plasma was collected, and neutrophils

were enriched by negative selection. Neutrophils from each cohort were used for bulk RNA sequencing (RNA-seq; n = 48) and neutrophil extracellular trap (NET) assays (spontaneous NET, n = 21, and microfluidics, n = 24); plasma was used for proteomics (n = 55) and cell-free DNA measurements (n = 63) (Figure 1; Table 1).

Transcriptional profiling of neutrophils from pediatric COVID-19 and MIS-C

To confirm the successful negative selection enrichment of neutrophils, we used a digital cytometry method, CIBERSORTx, to estimate the fractions of major cell-type lineages in each bulk RNA-seq sample.[16] We used the single-cell RNA-seq COVID-19 Bonn Cohort 2 reference dataset to generate cell-type-specific signatures for mature neutrophils, immature neutrophils, monocytes, T/natural killer (NK) cells, B cells, and plasmablasts.[4] The total neutrophil fraction was defined as the sum of mature and immature neutrophils. High purity of neutrophils was confirmed in all samples that passed quality control (Figure S1A; Table S3), and the majority of samples had high mature-to-immature neutrophil ratios. Notably, there were no significant differences in any CIBERSORTx fractions between the patient cohorts (Figure S1B). Additionally, flow cytometry confirmed high neutrophil purity with minimal monocyte and lymphocyte contamination (Figure S1C) and no eosinophil contamination (Figure S1D).

Uniform manifold approximation and projection (UMAP) visualization of bulk RNA-seq samples did not reveal distinct groupings based on patient cohort or CIBERSORTx-estimated cell-type percentages. Though we did not perform clustering analyses due to the small number of rare samples, the UMAP landscape was broadly characterized by two major groupings, which represent distinct transcriptional profiles (Figure S1E).

Acute COVID-19 infection is associated with neutrophil interferon response signatures in children

To identify differentially expressed genes and pathways in neutrophils associated with acute SARS-CoV-2 infection in children,
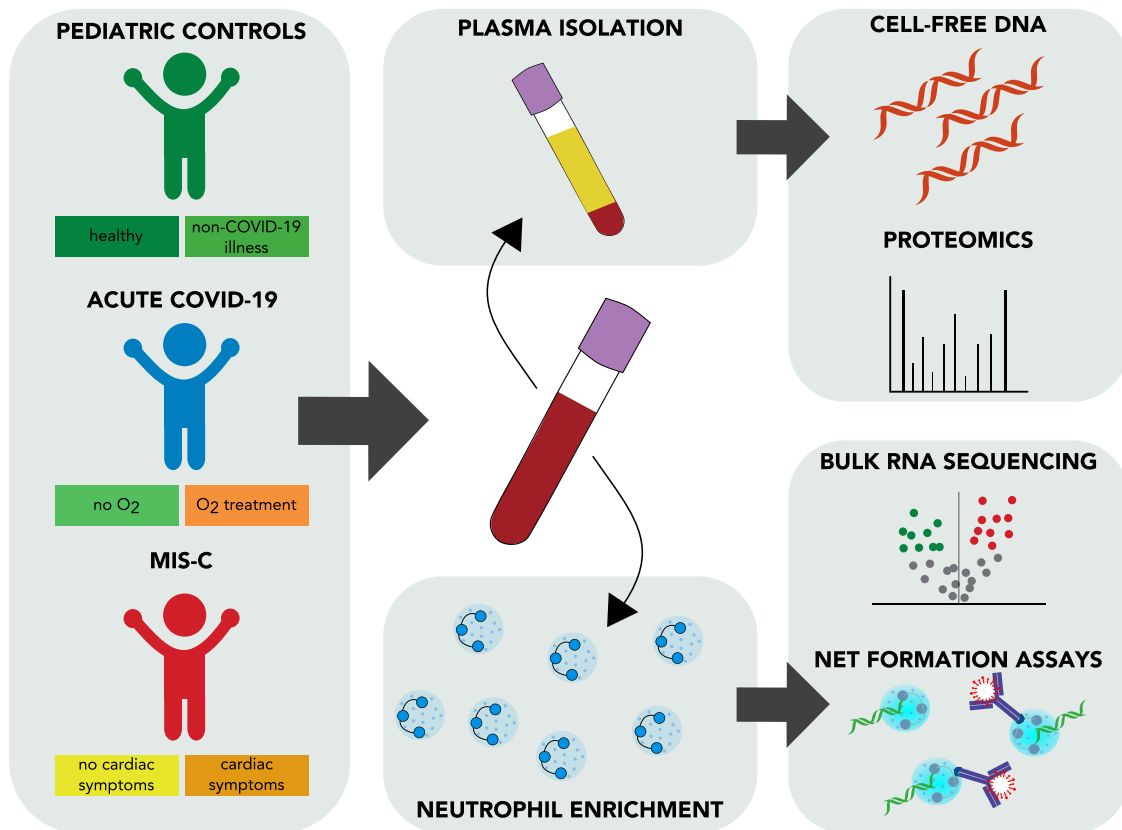
Figure 1. Overview of cohort and experimental schematic

Whole blood samples were collected from three cohorts: (1) pediatric healthy controls, (2) pediatric acute COVID-19 infection, and (3) multisystem inflammatory syndrome in children (MIS-C). Plasma collected from whole-blood samples was used in proteomic assays to quantify levels of protein and cell-free DNA. Isolated neutrophils were used in bulk RNA sequencing and NETosis assays. Patient samples were used in individual or multiple assays.

See also Figure S1 and Tables S1 and S2.

we performed differential expression analysis and gene set enrichment analysis (GSEA) between COVID-19-positive samples and healthy samples (Table S4). The most highly upregulated gene in COVID-19-positive samples was *CCRL2*, a gene critical for CXCR2-dependent neutrophil recruitment and β2-integrin activation[17] (Figure 2A). Following closely were other genes implicated in neutrophil chemotaxis, activation, and type I and II interferon responses such as *ELMO2*, *GPR84*, *IRF7*, *IFIT3*, and *MX1*. Overall, COVID-19-positive samples showed strong enrichment of pathways involved in antiviral response, including responses to interferon gamma (IFNγ) and IFNα (Figure 2B; Table S4).

In order to identify bulk neutrophil gene expression subtypes involved in response to SARS-CoV-2 infection in children, we utilized the bulk neutrophil gene signatures defined by an identical protocol in a large adult cohort,[1] as well as previously defined neutrophil signatures from single-cell and bulk RNA-seq data.[10,18] Pre-defined signatures included progenitor neutrophils (NMF1: Pro-Neu), nuclear factor κB (NF-κB)-activated neutrophils (NMF2: NF-κB+), IFN-stimulated neutrophils with high expression of PD-L1 (NMF3: PD-L1+ ISG+), immature activated neutrophils (NMF4: Immature), granulocytic myeloid-derived suppressor cell-like (G-MDSC) neutrophils (NMF5: G-MDSCs),

and a second IFN-stimulated neutrophil signature with lower expression of PD-L1 and a non-overlapping set of IFN-stimulated genes (ISGs) (NMF6: ISG+)[1,10,18] (Figure 2C). Since these signatures were also derived from bulk RNA-seq data, they represent transcriptional profiles of a mixture of neutrophil states rather than one specific subpopulation. When scoring each sample based on their average expression of NMF genes compared with their average expression of a control gene set (method details), we found that many of the NMF signatures produced groupings on the UMAP (Figure 2D), indicating the utility of these bulk signatures in defining neutrophil state signatures in children with COVID-19.

Next, we performed GSEAs comparing neutrophil subtype signature gene sets from children with COVID-19 and healthy controls (Table S4). Briefly, genes were ranked by signed log(p values) of the DESeq2 differential expression analysis between acute pediatric COVID-19 and healthy controls, and an enrichment score was calculated to indicate the degree to which the gene set was overrepresented at the top or bottom of the ranked list. We found significant enrichment of the NMF3: PD-L1+ ISG+ and the NMF6: ISG+ neutrophil subtypes in COVID-19 (Figure 2E), plus a weak enrichment for the NMF5: G-MDSC subtype in COVID-19. Conversely, the
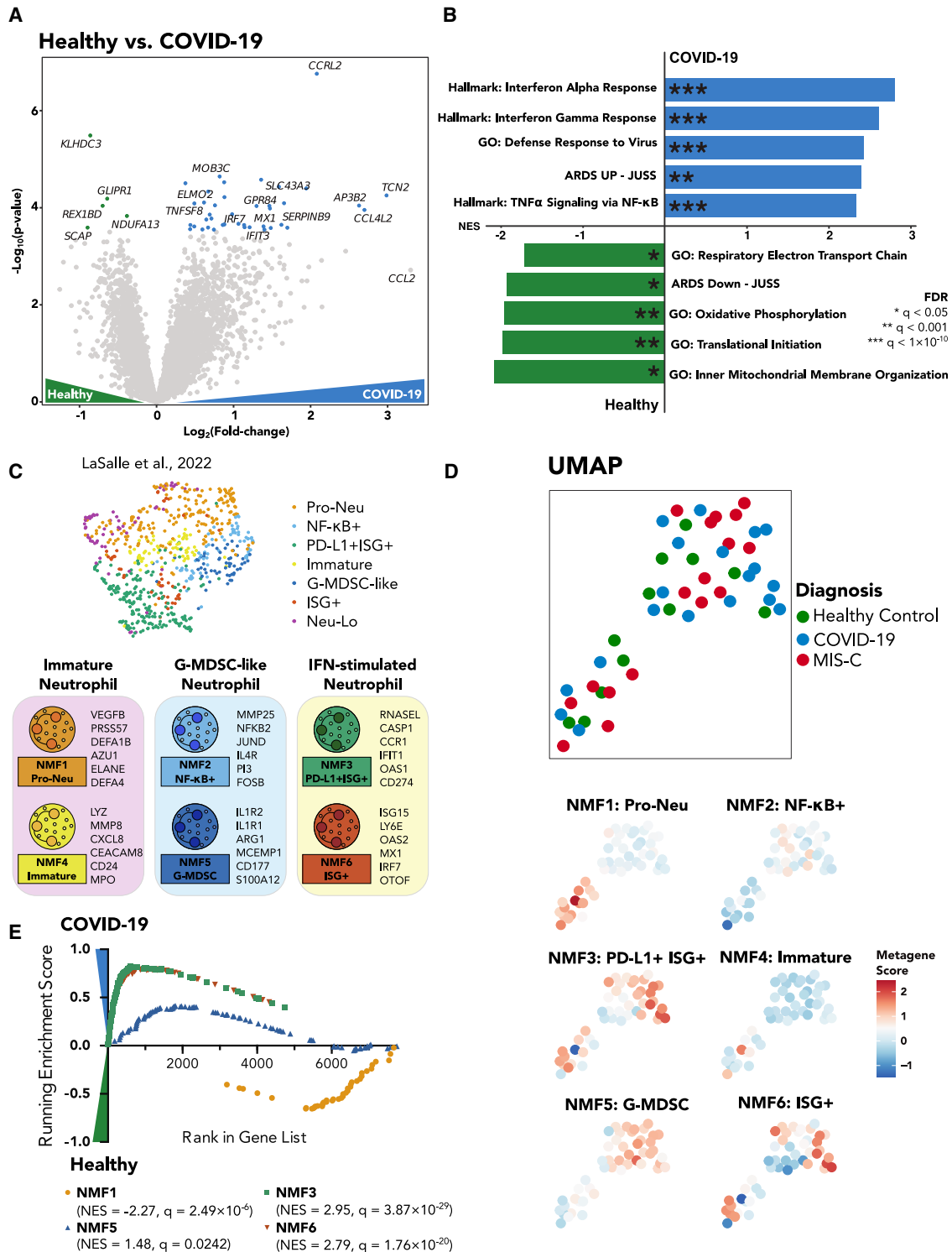
Figure 2. Acute pediatric COVID-19 neutrophils are marked by a robust interferon-stimulated gene signature

(A) Volcano plot showing differentially expressed genes between pediatric acute COVID-19 and healthy control samples. Color-coded points indicate genes that pass false discovery rate (FDR) correction with q < 0.05.

(B) Gene set enrichment analysis for the differentially expressed genes in (A). Bar lengths correspond to normalized enrichment score (NES), with positive NES values indicating enrichment in COVID-19 and negative values indicating enrichment in healthy pediatric controls. Asterisks denote significance as defined in the figure.

(legend continued on next page)

NMF1: Pro-Neu signature was slightly enriched in the healthy controls compared with pediatric COVID-19 (Figure 2E). Taken together, these results confirm that acute COVID-19 infection in children induces an ISG signature in neutrophils similar to early stages of infection in adults.[1]

MIS-C is associated with a strong G-MDSC signature having similarities to severe COVID-19 in adults and sepsis

To define neutrophil activation in MIS-C, we performed differential expression analysis and GSEAs comparing MIS-C samples with healthy pediatric controls (Table S4). The most highly upregulated gene in MIS-C neutrophils was *GPR84*, a gene involved in reactive oxygen species (ROS) production and neutrophil activation[19] (Figure 3A). Following closely was *ACER3*, a gene that has been shown to be upregulated in blood neutrophils of adult patients with ARDS, and several genes involved in glucose metabolism including *LDHA* and *ENO1* and the complement C3 receptor *C3AR1*, which may modulate neutrophil recruitment, were also elevated in neutrophils from patients with MIS-C.[20]

The most highly enriched pathway in MIS-C was ARDS Up - Juss, a collection of genes that were found to be upregulated at least 3-fold in adult ARDS blood neutrophils compared with healthy controls[10] (Figure 3B; Table S4). Accordingly, healthy control samples relative to MIS-C most prominently expressed the ARDS Down - Juss pathway, containing genes upregulated at least 3-fold in healthy controls over ARDS samples. In agreement with the top differentially expressed genes, the next most highly enriched pathways in MIS-C were oxidative phosphorylation, glycolysis, and mTORC1 signaling, suggesting that MIS-C neutrophils are highly metabolically active. Finally, MIS-C samples were also enriched for neutrophil degranulation, tumor necrosis factor (TNF) signaling, and interleukin-1 (IL-1) signaling, suggesting a mechanism by which neutrophils contribute to tissue damage in this highly inflammatory disease.

Next, we sought to determine which neutrophil subtypes were enriched in MIS-C. GSEA revealed a strong enrichment of the NMF5: G-MDSC subtype in MIS-C, the subtype that was most strongly associated with severe disease and death in adult patients with COVID-19[1,4,21] (Figure 3C; Table S4), and NMF4, suggesting that a proportion of patients with MIS-C may have high levels of a specific population of immature neutrophils (pre-neutrophils) that have been linked to increased NETosis, neutrophil degranulation, and activation.[1]

We performed a direct comparison of MIS-C and acute pediatric COVID-19 neutrophils to validate our findings from the individual healthy control comparisons (Table S4). Indeed, we observed a host of upregulated ISGs in acute COVID-19 that

vanish in MIS-C, suggesting that the acute antiviral response has subsided in this late stage of disease, and instead, we find several markers of increased cellular metabolism consistent with neutrophil activation (Figure S2A; Table S4). In agreement with these gene markers, the ISG+ neutrophil states (NMF3 and NMF6) were found to be consistently highly enriched in acute pediatric COVID-19, while immature, NETosis-associated, and G-MDSC states (NMF1, NMF4, and NMF5, respectively) were enriched in MIS-C, albeit with more heterogeneity (Figures S2B, S2C, and S3). We confirmed the enrichment of these states in acute pediatric COVID-19 versus MIS-C using a second gene set analysis technique called sigPathway[22] (Table S4; method details). Additional markers for pediatric acute COVID-19 and MIS-C are highlighted in Figure 3D.

Cardiac involvement is often associated with MIS-C but is not required for diagnosis; several patients in our cohort had either myocarditis, ventricular dysfunction, or coronary arterial aneurysm, with two patients requiring extracorporeal membrane oxygenation (ECMO). Thus, we next performed a hypothesis-generating differential expression analysis to identify neutrophilic transcriptional differences between patients with (n = 13) or without (n = 4) cardiac symptoms of MIS-C (Figure S3A). Several hallmark genes of sepsis and antigen presentation were enriched in cardiac MIS-C (Figure S3B), including several of the MHC II genes (*HLA-DQB1*, *HLA-DRA*, *HLA-DMB*). Other potential markers of severe cardiac MIS-C are *CD163*, which has been shown to be upregulated in PMNs of children with sepsis,[23] *ZBTB16*, which is high in adults with sepsis and severe COVID-19,[1,10] and *OLAH*, which is high in complex disease courses in sepsis.[24]

Neutrophils from children with MIS-C undergo high levels of spontaneous NETosis

As many of the highly upregulated genes and pathways from children with MIS-C are involved in neutrophil activation and potentially destructive neutrophil effector functions such as NET formation, granule release, and ROS production, we sought to verify that the findings from the gene expression analysis corresponded to functional changes in neutrophils. We visualized neutrophil activation by studying spontaneous NET formation by neutrophils from patients with MIS-C compared with those from healthy donors. NETs were observed by microscopy using microfluidic technology; Neutrophils stimulated with 100 nM phorbol myristate acetate (PMA), a known, potent stimulator of NET formation, served as a positive control.

Neutrophils were isolated immediately after phlebotomy, plated without any added stimulants or neutrophil activators, and visualized via time-lapse microscopy for 4 h (experimental

---

(C) UMAP of neutrophil bulk RNA sequencing (RNA-seq) samples from adults with acute COVID-19 and healthy controls from LaSalle et al.[1] UMAP is color coded by cluster designation. Bottom, schematic illustrating several top genes associated with each neutrophil subtype. Neu-Lo, samples excluded from clustering based on estimated low neutrophil fraction by CIBERSORTx.

(D) (Top) UMAP plots of neutrophil bulk RNA-seq data. Each point is one bulk sample, and points are color coded according to disease status. (Bottom) UMAPs of all neutrophil samples that were sequenced with bulk RNA-seq. Samples are colored according to their expression score of each neutrophil state metagene.

(E) GSEA enrichment plots for the NMF1 (Pro-Neu), NMF3 (PD-L1+ ISG+), NMF5 (G-MDSC), and NMF6 (ISG+) signatures, the four NMF neutrophil signatures that passed FDR correction. Each point represents one gene in the gene signature. Positive scores denote enrichment in acute pediatric COVID-19, and negative scores denote enrichment in healthy controls.
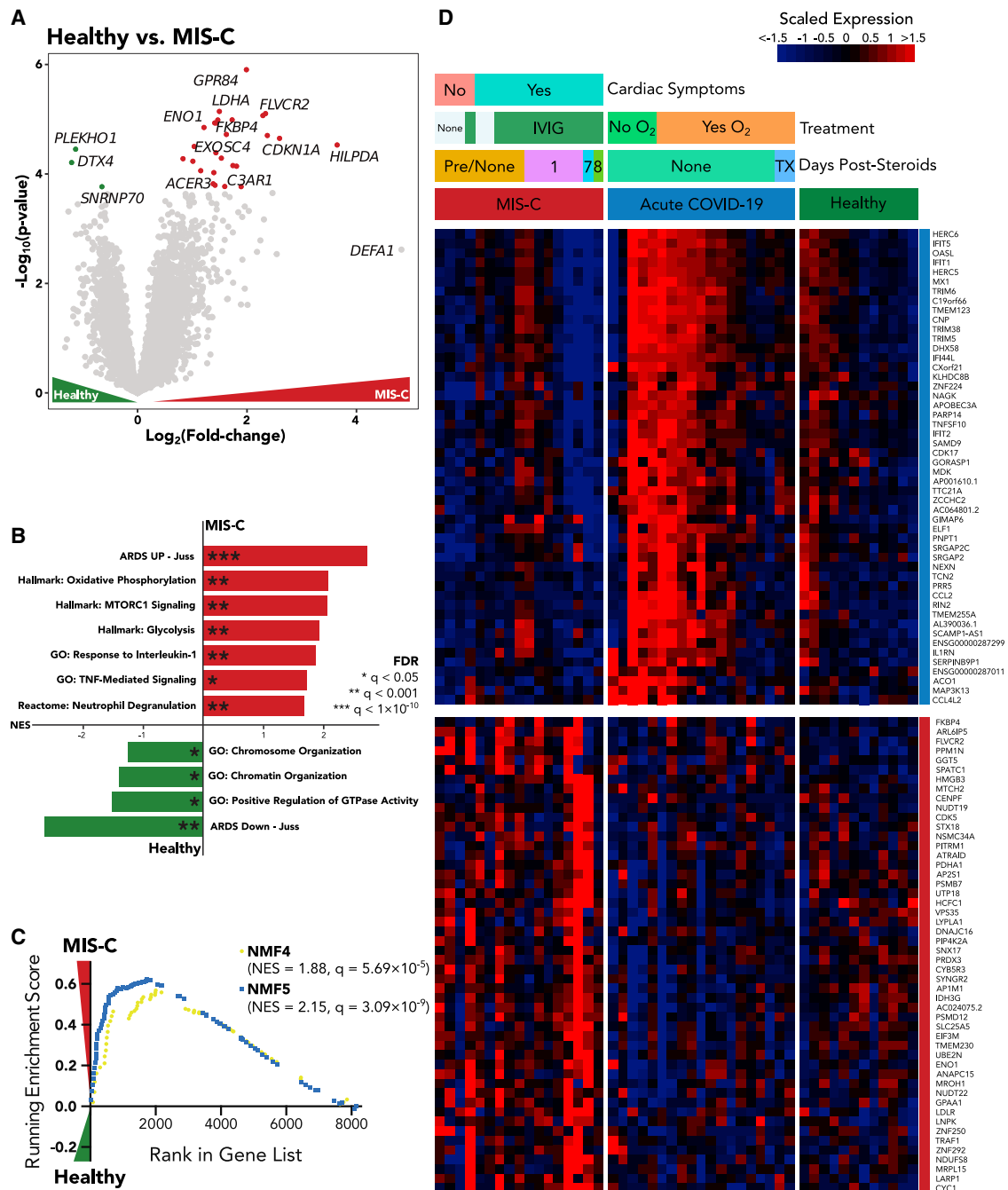
See also Tables S3, S4, and S5.

Figure 3. Neutrophils from patients with MIS-C display a strong G-MDSC signature and are characterized by altered metabolism

(A) Volcano plot showing differentially expressed genes between MIS-C and pediatric healthy control samples. Color-coded points indicate genes that pass FDR correction with q < 0.05.

(B) Gene set enrichment analysis for the differentially expressed genes in (A). Bar lengths correspond to NES, with positive NES values indicating enrichment in MIS-C and negative values indicating enrichment in healthy controls. Asterisks denote significance as defined in the figure.

(C) GSEA enrichment plots for the NMF4 (Immature) and NMF5 (G-MDSC) signatures, the two NMF neutrophil signatures that passed FDR correction.

(D) Heatmap displaying scaled RNA-seq expression values for gene markers distinguishing pediatric acute COVID-19 and MIS-C. The color coding on the right of the heatmap indicates whether the gene was differentially expressed in MIS-C versus COVID-19 and healthy or COVID-19 versus MIS-C or healthy. Color-coded bars above indicate disease status, cardiac involvement for patients with MIS-C, course of treatment, and days since the administration of steroids.

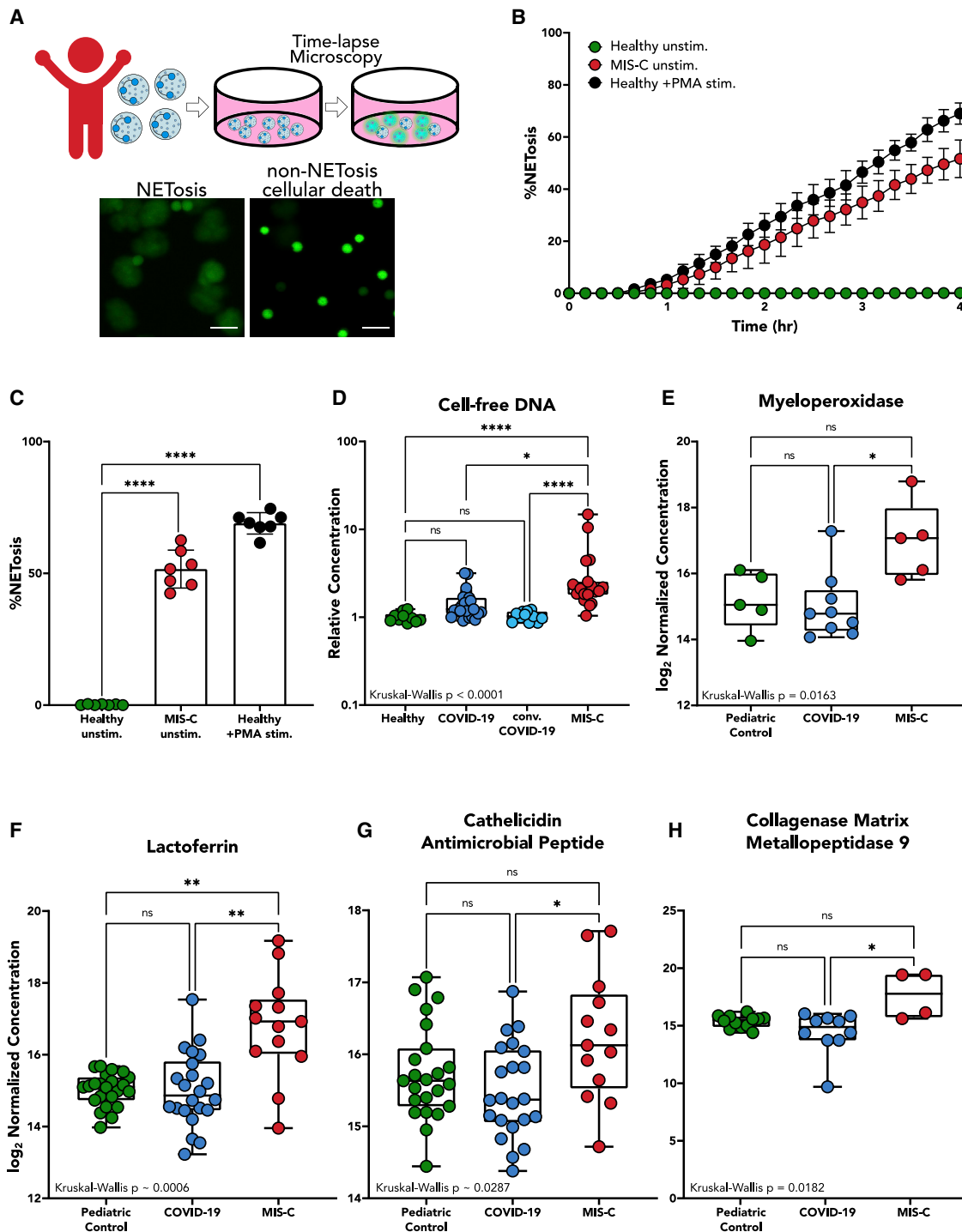See also Figures S2 and S3 and Tables S3, S4, and S5.

Figure 4. Fluorescence microscopy, cell-free DNA, and plasma protein markers implicate high levels of NETosis in MIS-C disease pathology

(A) Neutrophils were isolated from patients with MIS-C or healthy controls and plated on a 96-well plate without any stimulus to measure neutrophil activation via spontaneous NET release. Scale bar: 50 μM.

(B) Temporal dynamics of NET release in unstimulated neutrophils from healthy children (n = 7) and children with MIS-C (n = 7), as well as healthy neutrophils stimulated with 100 nM PMA (n = 7).

(C) End-point percentage of NETosis in unstimulated neutrophils from healthy children and children with MIS-C and healthy neutrophils stimulated with 100 nM PMA.

overview in Figure 4A). While neutrophils from healthy pediatric controls showed minimal spontaneous NETosis over the 4 h (Video S1, top), neutrophils isolated from children with MIS-C showed ∼500-fold higher rates of spontaneous NETosis (percentage of neutrophils undergoing NETosis: MIS-C 52% ± 7% versus healthy controls 0.17% ± 0.21%, p < 0.0001; Figures 4B and 4C; Video S1, bottom). The spontaneously formed NETs in MIS-C neutrophils were similar to PMA-stimulated NETs from healthy pediatric children, reaching markedly elevated levels of NET formation (69% ± 4% NETosis; Figures 4B and 4C).

To corroborate evidence of NETosis in MIS-C, we probed for markers of NET release. We found that children with MIS-C had significantly higher levels of relative cell-free DNA within their plasma compared to children with acute COVID-19, children with convalescent COVID-19 (p = 0.0160) and healthy children (p < 0.0001) (Figure 4D). Though cell-free DNA is non-specific and could come from other forms of cell death, recent studies showed that circulating cell-free DNA in severe adult COVID-19 is primarily derived from hematopoietic cells, specifically neutrophils.[25] We also used mass spectrometry to quantify levels of protein markers of NET release. When comparing plasma from children with acute COVID-19, MIS-C, and non-COVID-19 illnesses, significant differences were detected in levels of myeloperoxidase (MPO) (p = 0.0163); lactoferrin (p < 0.0182); collagenase matrix metallopeptidase 9 (MMP9) (p = 0.0006); and cathelicidin anti-microbial peptide (CAMP) (p = 0.0287) (Figures 4E–4H), with children with MIS-C displaying elevated levels of each of these enzymes in circulation.

Circulating anti-SARS-CoV-2 immune complexes stimulate NETosis

Current models of MIS-C pathogenesis suggest that the characteristic immune hyperactivation of the disease is driven by persistent circulating spike antigenemia[6] without viremia[26] months after the initial SARS-CoV-2 infection. In one study, viral persistence in the gastrointestinal (GI) tract led to the release of zonulin, a biomarker of intestinal permeability, which subsequently led to leakage of viral antigens into the bloodstream and subsequent immune hyperactivation.[6] Thus, we hypothesized that SARS-CoV-2 antigen:antibody immune complexes (ICs) could be responsible for triggering NETosis in the vasculature, contributing to cardiovascular pathology seen in MIS-C. To probe this mechanism of increased NET formation in children with MIS-C, neutrophils isolated from healthy controls were treated for 4 h with ICs generated by incubating patient-derived plasma with SARS-CoV-2 spike antigen (experimental overview, Figures 5A and S4). We observed low levels of NETosis when neutrophils were stimulated with spike antigen plus buffer (12% ± 3%; Figures 5B and 5C) or plasma from non-COVID-19

controls without spike antigen (12% ± 2%) and with spike antigen (14% ± 4%), likely due to the absence of spike-specific antibodies and ICs in these children (Figures 5B and 5C). We then stimulated neutrophils with convalescent COVID-19 plasma, both in the presence and in the absence of spike antigen, to determine if SARS-CoV-2 antibodies alone could induce NETosis, and we again observed low levels of NETs in these stimulated neutrophils (11% ± 3%; Figures 5B and 5C), indicating that neither antibodies nor antigen alone will induce NETosis.

However, the addition of spike antigen to convalescent COVID-19 plasma induced significant NETosis (30% ± 3%) (Video S2, top) compared with convalescent COVID-19 plasma alone (p < 0.0001) (Figures 5B and 5C). This level of NETosis was comparable with that seen when healthy neutrophils were stimulated with MIS-C plasma (30% ± 1%; Video S2, bottom). This increase in NET formation is likely due to the formation of SARS-CoV-2-specific antibody:antigen ICs in the sample. To further verify this claim, we added additional spike antigen to MIS-C plasma, which stimulated an even greater amount of NET formation (40% ± 8%; Figures 5B and 5C). Similarly, we found that plasma from healthy, vaccinated children alone did not stimulate neutrophils but that the exogenous addition of spike beads to their vaccine-generated antibodies stimulated NETosis (29% ± 5%; Figure S4). These results provide further evidence of circulating spike antigen in patients with MIS-C, which triggers the formation of inflammatory ICs and subsequent neutrophil activation.

To better understand which antibody class of anti-spike ICs was driving NETosis in MIS-C, we depleted either immunoglobulin G (IgG)-ICs, IgA-ICs, or both IgG- and IgA-ICs from MIS-C plasma and quantified NETosis. Compared with non-depleted MIS-C plasma (29% ± 5%), IgA depletion (14% ± 3%) resulted in the greatest decrease in NET formation (p < 0.0001), although IgG depletion (22% ± 3%) contributed to a lesser degree (p = 0.0145) (Figures 5D and 5E).

Together, these results suggest that SARS-CoV-2 antigenemia in the setting of a mature humoral response appears to instigate excessive neutrophil activation with hyperinflammatory and detrimental intravascular NET formation in MIS-C.

DISCUSSION

In this study, we report the first in-depth characterization of neutrophils in pediatric acute COVID-19 and MIS-C. Utilizing neutrophil bulk RNA-seq, plasma protein expression, and functional analyses of neutrophils, we highlight major differences in the neutrophil response that help to explain the divergent presentations of these SARS-CoV-2-related diseases and provide mechanistic insight into neutrophil activation by SARS-CoV-2 antigen:antibody ICs in MIS-C.

(D) Quantification of circulating cell-free DNA in plasma of healthy patients (n = 10), children with COVID-19 (n = 19), children with convalescent COVID-19 (n = 11), and children with MIS-C (n = 19). Displayed as fold increase from baseline (healthy controls).

(E–H) Peak values of myeloperoxidase (E), lactoferrin (F), cathelicidin antimicrobial peptide (G), and collagenase matrix metallopeptidase 9 (H) quantified in plasma from pediatric controls (n = 23), children with acute COVID-19 (n = 19), and children with MIS-C (n = 13).

(B) Mean values and SD are presented. (C) One-way ANOVA with multiple comparisons. Mean values and SD are presented. (D)–(H) Median values are shown with interquartile ranges; significance was determined by Kruskal-Wallis. Statistical significance is defined as *p < 0.05, **p < 0.01, ***p < 0.001, and ****p < 0.0001. See also Video S1.
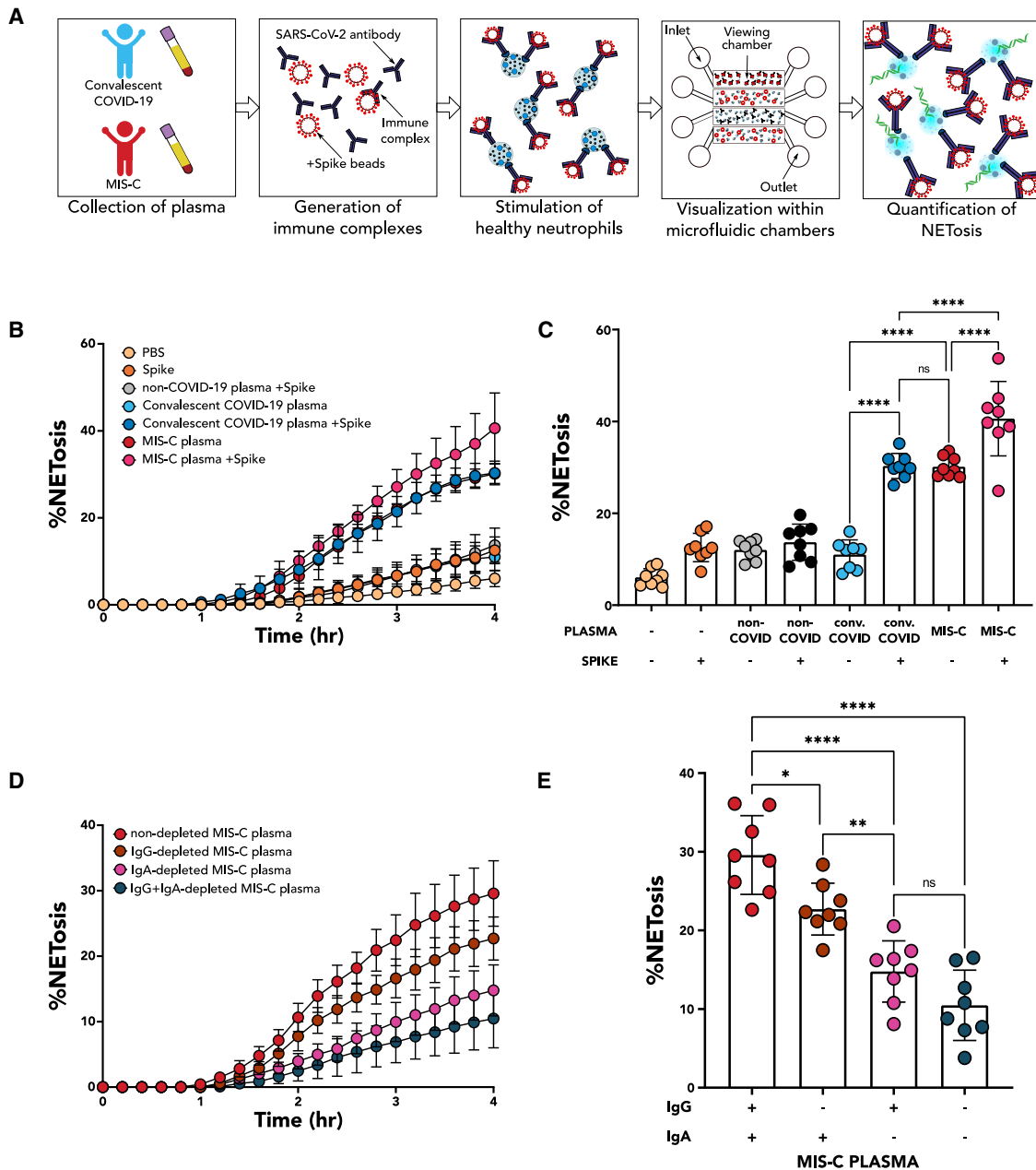
Figure 5. SARS-CoV-2 spike immune complexes trigger NETosis

(A) Plasma was collected from several children with non-COVID-19 illness, convalescent COVID-19, and MIS-C and pooled together. Pooled plasma was diluted at 1:10 and incubated with beads coated with spike proteins to generate immune complexes or without the presence of spike protein to measure the stimulation of plasma alone. Neutrophils were isolated from healthy children, stimulated, and visualized within four viewing channels of a microfluidic device.

(B) Temporal dynamics of NET release in neutrophils (n = 8) stimulated with PBS, PBS-treated spike beads, non-COVID-19 plasma, non-COVID-19-plasma-coated spike beads, convalescent COVID-19 plasma, convalescent COVID-19-plasma-coated spike beads, MIS-C plasma, and MIS-C-plasma-coated spike beads.

(C) End-point percentage of NET release in neutrophils (n = 8) stimulated with conditions described in (B).

(D) Temporal dynamics of NET release in neutrophils (n = 8) stimulated with non-depleted MIS-C plasma, IgG-depleted MIS-C plasma, IgA-depleted MIS-C plasma, and MIS-C plasma depleted of both IgG and IgA.

(E) End-point percentage of NET release in neutrophils (n = 8) stimulated with plasma as described in (D).

(B–E) Mean values and SD are presented. (C and D) Significance was determined by one-way ANOVA with multiple comparisons. Statistical significance is defined as *p < 0.05, **p < 0.01, ***p < 0.001, and ****p < 0.0001.
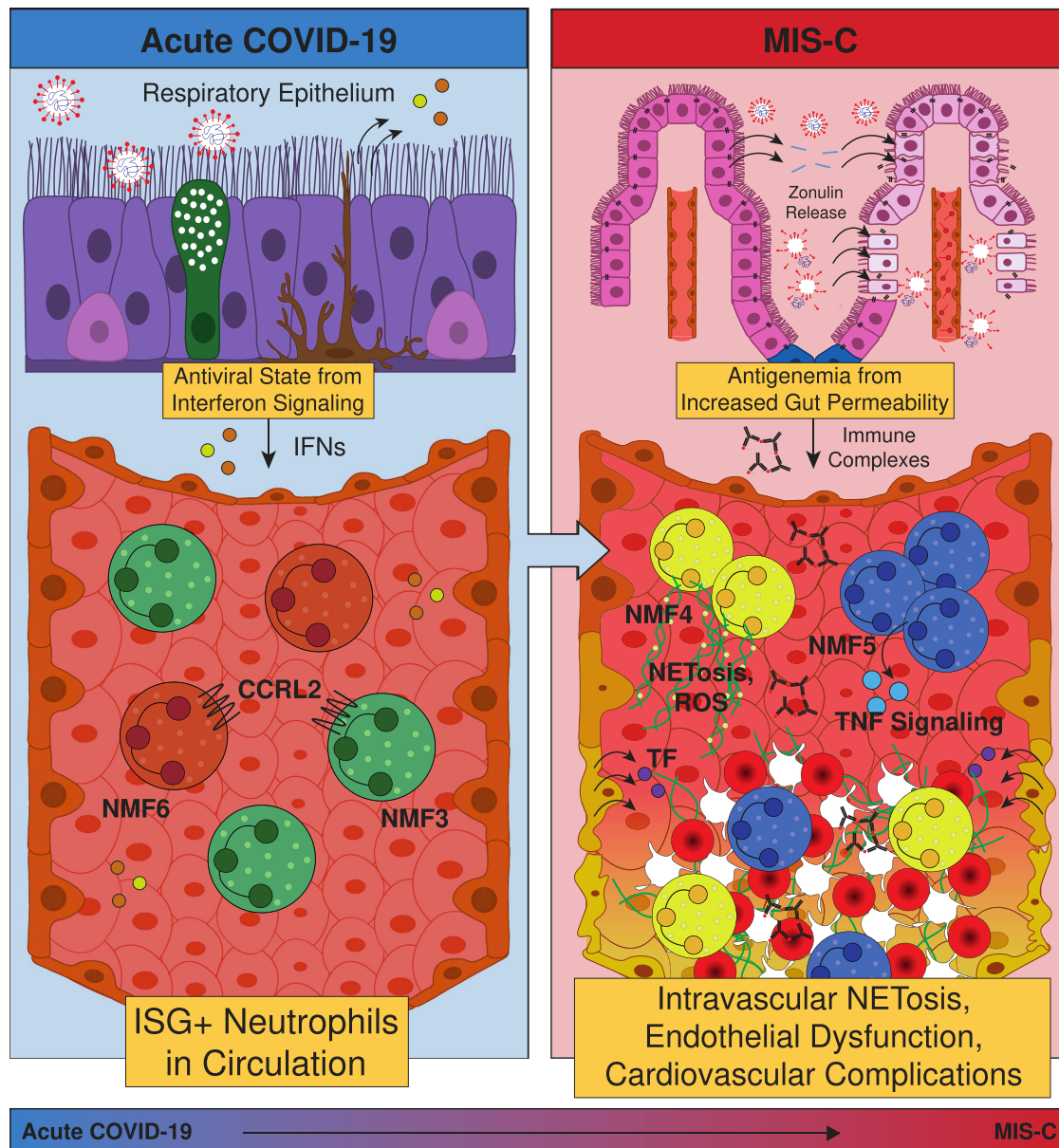
See also Figures S4 and S5 and Videos S2 and S3.

Figure 6. Schematic of the role of neutrophils in pediatric COVID-19 and MIS-C
Acute SARS-CoV-2 infection begins in the respiratory epithelium, and interferon signaling induces ISG+ neutrophils in circulation. Weeks later, viral persistence in the gut lumen results in zonulin release from gut epithelial cells, leading to loss of tight junctions and SARS-CoV-2 antigen leakage. Finally, immune complexes trigger NETosis and induce G-MDSCs, resulting in endothelial dysfunction and cardiovascular complications.

MIS-C, though SARS-CoV-2-related, presents as a completely distinct set of symptoms and neutrophil phenotypes from acute COVID-19 in both children, shown here, and previous reports in adults.[1] MIS-C occurs weeks to months after the initial infection, with a notable absence of viremia,[26] in contrast to acute severe COVID-19.[27] Instead, MIS-C is linked to SARS-CoV-2 antigenemia without replication-competent virus in a mature humoral response setting. Studies have demonstrated that viral RNA is still detected in the stool weeks after infection or exposure.[6,28] In children who develop MIS-C, viral persistence is associated with increased gut permeability through zonulin release by gut epithelial cells,[6] allowing viral antigens to escape into the bloodstream, where primed antibodies await. The formation of ICs triggers a hyperinflammatory immune response with neutrophil activation and NET formation within the vasculature (Figure 6).

As a result of this distinct mechanism, neutrophils in MIS-C are characterized by upregulated genes and pathways associated with G-MDSCs and the formation of NETs, which is highly distinct from the antiviral gene signature seen in acute pediatric COVID-19. Neutrophils in patients with MIS-C more closely

resemble those found in patients with non-viral ARDS[10] or sepsis,[21] rather than mild acute COVID-19, in that they appear to take on an immature, T cell-suppressive phenotype. This activated and destructive phenotype is hypothesized to cause the systemic damage seen in patients with MIS-C, with potential mechanisms being the interaction of neutrophil Fc receptors with SARS-CoV-2 antigen ICs, or TNF-α signaling via NF-κB, which in excess can dysregulate T cells[29] or activate further NETosis. Indeed, increased NF-κB signaling has been shown to be upregulated in monocytes and dendritic cells in MIS-C, especially in severe cardiac MIS-C,[30] but prior reports have not examined neutrophils. Activated neutrophils have been implicated in the pathology of myocarditis through infiltration into the heart, with evidence of NETs found in endomyocardial biopsies from patients with myocarditis.[31–33] As activated neutrophils and viral particles have been found in the myocardium postmortem in patients with MIS-C,[34,35] increased antigen presentation by neutrophils and upregulation of septic responses by neutrophils may play a role in pathology driving severe cardiac complications of MIS-C. Importantly, this neutrophil activation can modulate B cell function, promoting autoimmune processes and contributing to immune activation in MIS-C[36] and potentially long COVID-19.[37] The role of the neutrophils in autoimmunity has already been established in conditions like anti-neutrophil cytoplasmic antibody-associated (ANCA-associated) vasculitis, Behcet's disease, and systemic lupus erythematosus.[38]

In this study, we also provide visual evidence of high rates of spontaneous NETosis in neutrophils from children with MIS-C with imaging experiments performed within hours of fresh whole-blood collection. Furthermore, we provide mechanistic insight into the abundant NET formation by showing that SARS-CoV-2 antigen:patient-derived antibody ICs, predominantly anti-spike IgA-ICs, can trigger NETosis in healthy donor neutrophils. While IgA plays a key role in neutralizing SARS-CoV-2 at the mucosal surface,[39] increased levels of IgA in circulation have been associated with severe COVID-19 in adults, with a corresponding increase in neutrophilic inflammatory responses.[40,41] IgA can be a potent inducer and potentiator of NET formation[42,43] but has not previously been implicated in MIS-C pathogenesis.

The observed NETosis has several implications for the disease pathology observed in MIS-C. Although NETs are effective at capturing and destroying pathogens at mucosal barriers, they can be a source of excessive inflammation and coagulation when released in circulation. First, NET components such as MPO can generate ROS and directly damage endothelium through several mechanisms, leading to tissue factor (TF) release. NETs themselves often contain TFs;[44] thus, both NETs and the damaged endothelium can initiate the extrinsic coagulation cascade. Second, the abundant extracellular DNA can serve as a damage-associated molecular pattern (DAMP),[45] triggering additional inflammation alongside inflammatory cytokine production, and the negative charge can initiate the intrinsic coagulation cascade.[46] Taken together, these mechanisms can serve as a scaffold for platelets, induce hypercoagulability and endothelial dysfunction and lead to thrombosis, vasculitis, and cardiovascular complications, providing a uniting framework for MIS-C pathogenesis (Figure 6).

Neutrophil activation in MIS-C starkly contrasts the ISG profile seen in neutrophils from children with acute COVID-19. In children, the antiviral response to SARS-CoV-2 is sufficient to clear the acute infection without severe symptoms, as evidenced by the mild or asymptomatic presentations in most cases. While live, infectious SARS-CoV-2 can be detected in the upper airways of children,[47] accounting for the antiviral response, there is little to no viremia detected in pediatric COVID-19.[26] This picture may be similar to that seen in adults with mild COVID-19. However, in adults with moderate to severe disease, impaired antiviral signaling can lead to viremia in a larger fraction of cases, resulting in a more severe presentation of acute COVID-19 in these individuals.[48–50] Thus, containment of the virus in the upper respiratory tract in children likely prevents the progression to more severe circulating neutrophil phenotypes seen in life-threatening COVID-19 in adults, and it is unlikely that circulating neutrophils alone determine disease severity in acute pediatric COVID-19.

There is an increasing appreciation of neutrophil activation in severe COVID-19 in adults, and therapies are being designed to target neutrophil hyperactivation. However, in most children, their immune system can already manage SARS-CoV-2 due to a strong IFN-mediated antiviral response.[14,15] In both adults and children, SARS-CoV-2 viremia or antigenemia and the resultant ICs appear to be responsible for deleterious NET formation. While therapies blunting excessive neutrophil activation could improve clinical outcomes in severe disease, mitigating the antigenemia or viremia will be critical. Previous studies have indicated that preventing SARS-CoV-2 antigen leakage from the gut with the zonulin antagonist larazotide may be effective in preventing antigenemia-included hyperinflammation in MIS-C.[6,51] While vaccination and avoidance of infection are the best prevention strategies, if SARS-CoV-2 infection does occur and MIS-C ensues, future studies may explore combination therapies that both prevent antigenemia by enhancing tight junctions in gut epithelium and simultaneously inhibiting systemic NET formation to improve upon the current treatment paradigm.

In summary, our study provides much-needed mechanistic insight into the drivers of pathology in MIS-C and its departure from mild acute SARS-CoV-2 infection in children. We link existing knowledge of gut mucosal breakdown and antigenemia in MIS-C to increased IC-dependent NETosis and a shift away from the antiviral state toward a sepsis-like G-MDSC phenotype, highlighting potential connections between neutrophil activation and the characteristic cardiovascular pathology to suggest pathways of intervention to improve the standard of care.

Limitations of the study
We acknowledge several limitations of our study. First, because of the nature of the pandemic and logistics around sample collection and processing of neutrophils, we chose to utilize bulk transcriptomics due to the technical challenges of performing single-cell RNA-seq on neutrophils, so each sample represents a mixture of neutrophils with distinct gene expression programs. However, our high-purity double isolation method left little contamination with other cell types. Second, we acknowledge the small cohort size, although it represents the largest cohort of its kind, due to the low incidence rate of the disease.

Third, based on the sample size limitation, we were unable to define new gene expression states that may have been specific to pediatric neutrophils and had to rely on the adult-derived signatures. However, that work demonstrated a relatively small set of conserved neutrophil states across many different disease contexts. Relatedly, we used GSEA to determine the enrichment of these previously defined states. This method can only indicate relative enrichment and may overestimate effect sizes; however, it currently remains an integral component of RNA-seq analysis. Fourth, MIS-C can present heterogeneously, and there was a mixture of treatment regimens and disease duration among the patients, which may have resulted in greater heterogeneity in the gene expression profiles. Fifth, we acknowledge that the concentration of spike protein used to elicit NETosis may not directly align with levels of antigenemia in patients with MIS-C; however, these spike beads allowed us to test the impact of ICs on neutrophil activation. All limitations considered, numerous technical challenges and time-sensitive issues were overcome in this study to allow for deep characterization of neutrophil profiles in acute pediatric COVID-19 and MIS-C, which can guide future studies, including utilizing single-cell technologies.

STAR★METHODS

Detailed methods are provided in the online version of this paper and include the following:

- KEY RESOURCES TABLE
- RESOURCE AVAILABILITY
  - Lead contact
  - Materials availability
  - Data and code availability
- EXPERIMENTAL MODEL AND SUBJECT DETAILS
  - MGH patient cohort description
- METHOD DETAILS
  - Neutrophil isolation and lysis
  - Validation of isolated neutrophil purity
  - Patient matched plasma isolation
  - Smart-Seq2 cDNA preparation
  - Library construction and sequencing
  - Spontaneous NET release fluorescence microscopy data acquisition
  - Cell-free DNA quantification
  - Plasma protein measurement
  - Design and fabrication of the microfluidic devices
  - Immune complex generation
  - Plasma IgG and IgA depletion
  - NETosis assay
- QUANTIFICATION AND STATISTICAL ANALYSIS
  - RNA-seq alignment
  - Quality control
  - Neutrophil fraction estimation and contamination control
  - Dimensionality reduction and visualization
  - Differential expression analysis
  - Gene set enrichment analysis and sigPathway
  - Sample pathway scoring
  - Disease marker gene selection and heatmap
  - Quantification of NETosis
  - Statistical analysis

REFERENCES

1. LaSalle, T.J., Gonye, A.L.K., Freeman, S.S., Kaplonek, P., Gushterova, I., Kays, K.R., Manakongtreecheep, K., Tantivit, J., Rojas-Lopez, M., Russo, B.C., et al. (2022). Longitudinal characterization of circulating neutrophils

uncovers phenotypes associated with severity in hospitalized COVID-19 patients. Cell Rep. Med. *3*, 100779. https://doi.org/10.1016/j.xcrm.2022.100779.

2. Aschenbrenner, A.C., Mouktaroudi, M., Krämer, B., Oestreich, M., Antonakos, N., Nuesch-Germano, M., Gkizeli, K., Bonaguro, L., Reusch, N., Baßler, K., et al. (2021). Disease severity-specific neutrophil signatures in blood transcriptomes stratify COVID-19 patients. Genome Med. *13*, 7. https://doi.org/10.1186/s13073-020-00823-5.

3. Meizlish, M.L., Pine, A.B., Bishai, J.D., Goshua, G., Nadelmann, E.R., Simonov, M., Chang, C.H., Zhang, H., Shallow, M., Bahel, P., et al. (2021). A neutrophil activation signature predicts critical illness and mortality in COVID-19. Blood Adv. *5*, 1164–1177. https://doi.org/10.1182/bloodadvances.2020003568.

4. Schulte-Schrepping, J., Reusch, N., Paclik, D., Baßler, K., Schlickeiser, S., Zhang, B., Krämer, B., Krammer, T., Brumhard, S., Bonaguro, L., et al. (2020). Severe COVID-19 is marked by a dysregulated myeloid cell compartment. Cell *182*, 1419–1440.e23, e1423. https://doi.org/10.1016/j.cell.2020.08.001.

5. CDC (2021). Information for Healthcare Providers about Multisystem Inflammatory Syndrome in Children (MIS-C). https://www.cdc.gov/mis/mis-c/hcp/index.html.

6. Yonker, L.M., Gilboa, T., Ogata, A.F., Senussi, Y., Lazarovits, R., Boribong, B.P., Bartsch, Y.C., Loiselle, M., Rivas, M.N., Porritt, R.A., et al. (2021). Multisystem inflammatory syndrome in children is driven by zonulin-dependent loss of gut mucosal barrier. J. Clin. Invest. *131*, 149633. https://doi.org/10.1172/jci149633.

7. Feldstein, L.R., Tenforde, M.W., Friedman, K.G., Newhams, M., Rose, E.B., Dapul, H., Soma, V.L., Maddux, A.B., Mourani, P.M., Bowens, C., et al. (2021). Characteristics and outcomes of US children and adolescents with multisystem inflammatory syndrome in children (MIS-C) compared with severe acute COVID-19. JAMA *325*, 1074–1087. https://doi.org/10.1001/jama.2021.2091.

8. Meghraoui-Kheddar, A., Chousterman, B.G., Guillou, N., Barone, S.M., Granjeaud, S., Vallet, H., Corneau, A., Guessous, K., de Roquetaillade, C., Boissonnas, A., et al. (2022). Two new neutrophil subsets define a discriminating sepsis signature. Am. J. Respir. Crit. Care Med. *205*, 46–59. https://doi.org/10.1164/rccm.202104-1027OC.

9. Zhang, Y., Wang, Q., Mackay, C.R., Ng, L.G., and Kwok, I. (2022). Neutrophil subsets and their differential roles in viral respiratory diseases. J. Leukoc. Biol. *111*, 1159–1173. https://doi.org/10.1002/jlb.1mr1221-345r.

10. Juss, J.K., House, D., Amour, A., Begg, M., Herre, J., Storisteanu, D.M.L., Hoenderdos, K., Bradley, G., Lennon, M., Summers, C., et al. (2016). Acute respiratory distress syndrome neutrophils have a distinct phenotype and are resistant to phosphoinositide 3-kinase inhibition. Am. J. Respir. Crit. Care Med. *194*, 961–973. https://doi.org/10.1164/rccm.201509-1818OC.

11. Pastorek, M., Dúbrava, M., and Celec, P. (2022). On the origin of neutrophil extracellular traps in COVID-19. Front. Immunol. *13*, 821007. https://doi.org/10.3389/fimmu.2022.821007.

12. Gómez-Moreno, D., Adrover, J.M., and Hidalgo, A. (2018). Neutrophils as effectors of vascular inflammation. Eur. J. Clin. Invest. *48*, e12940. https://doi.org/10.1111/eci.12940.

13. Hsieh, L.E., Grifoni, A., Sidney, J., Shimizu, C., Shike, H., Ramchandar, N., Moreno, E., Tremoulet, A.H., Burns, J.C., and Franco, A. (2021). Characterization of SARS-CoV-2 and common cold coronavirus-specific T-cell responses in MIS-C and Kawasaki disease children. Eur. J. Immunol. *52*, 123–137. https://doi.org/10.1002/eji.202149556.

14. Ravichandran, S., Tang, J., Grubbs, G., Lee, Y., Pourhashemi, S., Hussaini, L., Lapp, S.A., Jerris, R.C., Singh, V., Chahroudi, A., et al. (2021). SARS-CoV-2 immune repertoire in MIS-C and pediatric COVID-19. Nat. Immunol. *22*, 1452–1464. https://doi.org/10.1038/s41590-021-01051-8.

15. Vella, L., Giles, J.R., Baxter, A.E., Oldridge, D.A., Diorio, C., Kuri-Cervantes, L., Alanio, C., Pampena, M.B., Wu, J.E., Chen, Z., et al. (2020). Deep Immune Profiling of MIS-C demonstrates marked but transient immune activation compared to adult and pediatric COVID-19. Preprint at medRxiv. https://doi.org/10.1101/2020.09.25.20201863.

16. Newman, A.M., Steen, C.B., Liu, C.L., Gentles, A.J., Chaudhuri, A.A., Scherer, F., Khodadoust, M.S., Esfahani, M.S., Luca, B.A., Steiner, D., et al. (2019). Determining cell type abundance and expression from bulk tissues with digital cytometry. Nat. Biotechnol. *37*, 773–782. https://doi.org/10.1038/s41587-019-0114-2.

17. Del Prete, A., Martínez-Muñoz, L., Mazzon, C., Toffali, L., Sozio, F., Za, L., Bosisio, D., Gazzurelli, L., Salvi, V., Tiberio, L., et al. (2017). The atypical receptor CCRL2 is required for CXCR2-dependent neutrophil recruitment and tissue damage. Blood *130*, 1223–1234. https://doi.org/10.1182/blood-2017-04-777680.

18. Zilionis, R., Engblom, C., Pfirschke, C., Savova, V., Zemmour, D., Saatcioglu, H.D., Krishnan, I., Maroni, G., Meyerovitz, C.V., Kerwin, C.M., et al. (2019). Single-cell transcriptomics of human and mouse lung cancers reveals conserved myeloid populations across individuals and species. Immunity *50*, 1317–1334.e10. https://doi.org/10.1016/j.immuni.2019.03.009.

19. Sundqvist, M., Christenson, K., Holdfeldt, A., Gabl, M., Mårtensson, J., Björkman, L., Dieckmann, R., Dahlgren, C., and Forsman, H. (2018). Similarities and differences between the responses induced in human phagocytes through activation of the medium chain fatty acid receptor GPR84 and the short chain fatty acid receptor FFA2R. Biochim. Biophys. Acta. Mol. Cell Res. *1865*, 695–708. https://doi.org/10.1016/j.bbamcr.2018.02.008.

20. Metzemaekers, M., Gouwy, M., and Proost, P. (2020). Neutrophil chemoattractant receptors in health and disease: double-edged swords. Cell. Mol. Immunol. *17*, 433–450. https://doi.org/10.1038/s41423-020-0412-0.

21. Reyes, M., Filbin, M.R., Bhattacharyya, R.P., Sonny, A., Mehta, A., Billman, K., Kays, K.R., Pinilla-Vera, M., Benson, M.E., Cosimi, L.A., et al. (2021). Plasma from patients with bacterial sepsis or severe COVID-19 induces suppressive myeloid cell production from hematopoietic progenitors in vitro. Sci. Transl. Med. *13*, eabe9599. https://doi.org/10.1126/scitranslmed.abe9599.

22. Tian, L., Greenberg, S.A., Kong, S.W., Altschuler, J., Kohane, I.S., and Park, P.J. (2005). Discovering statistically significant pathways in expression profiling studies. Proc. Natl. Acad. Sci. USA *102*, 13544–13549. https://doi.org/10.1073/pnas.0506577102.

23. Groselj-Grenc, M., Ihan, A., and Derganc, M. (2008). Neutrophil and monocyte CD64 and CD163 expression in critically ill neonates and children with sepsis: comparison of fluorescence intensities and calculated indexes. Mediators Inflamm. *2008*, 202646. https://doi.org/10.1155/2008/202646.

24. Banerjee, S., Mohammed, A., Wong, H.R., Palaniyar, N., and Kamaleswaran, R. (2021). Machine learning identifies complicated sepsis course and subsequent mortality based on 20 genes in peripheral blood immune cells at 24 H post-ICU admission. Front. Immunol. *12*, 592303. https://doi.org/10.3389/fimmu.2021.592303.

25. Andargie, T.E., Tsuji, N., Seifuddin, F., Jang, M.K., Yuen, P.S., Kong, H., Tunc, I., Singh, K., Charya, A., Wilkins, K., et al. (2021). Cell-free DNA maps COVID-19 tissue injury and risk of death and can cause tissue injury. JCI Insight *6*, 147610. https://doi.org/10.1172/jci.insight.147610.

26. Yonker, L.M., Neilan, A.M., Bartsch, Y., Patel, A.B., Regan, J., Arya, P., Gootkind, E., Park, G., Hardcastle, M., St John, A., et al. (2020). Pediatric severe acute respiratory syndrome coronavirus 2 (SARS-CoV-2): clinical presentation, infectivity, and immune responses. J. Pediatr. *227*, 45–52.e5, e45. https://doi.org/10.1016/j.jpeds.2020.08.037.

27. Fajnzylber, J., Regan, J., Coxen, K., Corry, H., Wong, C., Rosenthal, A., Worrall, D., Giguel, F., Piechocka-Trocha, A., Atyeo, C., et al. (2020). SARS-CoV-2 viral load is associated with increased disease severity and mortality. Nat. Commun. *11*, 5493. https://doi.org/10.1038/s41467-020-19057-5.

28. Natarajan, A., Zlitni, S., Brooks, E.F., Vance, S.E., Dahlen, A., Hedlin, H., Park, R.M., Han, A., Schmidtke, D.T., Verma, R., et al. (2022). Gastrointestinal symptoms and fecal shedding of SARS-CoV-2 RNA suggest

prolonged gastrointestinal infection. Med 3, 371–387.e9, e379. https://doi.org/10.1016/j.medj.2022.04.001.

29. Mehta, A.K., Gracias, D.T., and Croft, M. (2018). TNF activity and T cells. Cytokine 101, 14–18. https://doi.org/10.1016/j.cyto.2016.08.003.

30. de Cevins, C., Luka, M., Smith, N., Meynier, S., Magérus, A., Carbone, F., García-Paredes, V., Barnabei, L., Batignes, M., Boullé, A., et al. (2021). A monocyte/dendritic cell molecular signature of SARS-CoV-2-related multisystem inflammatory syndrome in children with severe myocarditis. Med (N Y) 2, 1072–1092.e7, e1077. https://doi.org/10.1016/j.medj.2021.08.002.

31. Müller, I., Vogl, T., Pappritz, K., Miteva, K., Savvatis, K., Rohde, D., Most, P., Lassner, D., Pieske, B., Kühl, U., et al. (2017). Pathogenic role of the damage-associated molecular patterns S100A8 and S100A9 in coxsackievirus B3-induced myocarditis. Circ. Heart Fail. 10, e004125. https://doi.org/10.1161/circheartfailure.117.004125.

32. Tschöpe, C., Ammirati, E., Bozkurt, B., Caforio, A.L.P., Cooper, L.T., Felix, S.B., Hare, J.M., Heidecker, B., Heymans, S., Hübner, N., et al. (2021). Myocarditis and inflammatory cardiomyopathy: current evidence and future directions. Nat. Rev. Cardiol. 18, 169–193. https://doi.org/10.1038/s41569-020-00435-x.

33. Weckbach, L.T., Grabmaier, U., Uhl, A., Gess, S., Boehm, F., Zehrer, A., Pick, R., Salvermoser, M., Czermak, T., Pircher, J., et al. (2019). Midkine drives cardiac inflammation by promoting neutrophil trafficking and NETosis in myocarditis. J. Exp. Med. 216, 350–368. https://doi.org/10.1084/jem.20181102.

34. Dolhnikoff, M., Ferreira Ferranti, J., de Almeida Monteiro, R.A., Duarte-Neto, A.N., Soares Gomes-Gouvêa, M., Viu Degaspare, N., Figueiredo Delgado, A., Montanari Fiorita, C., Nunes Leal, G., Rodrigues, R.M., et al. (2020). SARS-CoV-2 in cardiac tissue of a child with COVID-19-related multisystem inflammatory syndrome. Lancet. Child Adolesc. Health 4, 790–794. https://doi.org/10.1016/s2352-4642(20)30257-1.

35. Duarte-Neto, A.N., Caldini, E.G., Gomes-Gouvêa, M.S., Kanamura, C.T., de Almeida Monteiro, R.A., Ferranti, J.F., Ventura, A.M.C., Regalio, F.A., Fiorenzano, D.M., Gibelli, M.A.B.C., et al. (2021). An autopsy study of the spectrum of severe COVID-19 in children: from SARS to different phenotypes of MIS-C. EClinicalMedicine 35, 100850. https://doi.org/10.1016/j.eclinm.2021.100850.

36. Porritt, R.A., Binek, A., Paschold, L., Rivas, M.N., McArdle, A., Yonker, L.M., Alter, G., Chandnani, H.K., Lopez, M., Fasano, A., et al. (2021). The autoimmune signature of hyperinflammatory multisystem inflammatory syndrome in children. J. Clin. Invest. 131, e151520. https://doi.org/10.1172/jci151520.

37. Noval Rivas, M., Porritt, R.A., Cheng, M.H., Bahar, I., and Arditi, M. (2022). Multisystem inflammatory syndrome in children and long COVID: the SARS-CoV-2 viral superantigen hypothesis. Front. Immunol. 13, 941009. https://doi.org/10.3389/fimmu.2022.941009.

38. Thieblemont, N., Wright, H.L., Edwards, S.W., and Witko-Sarsat, V. (2016). Human neutrophils in auto-immunity. Semin. Immunol. 28, 159–173. https://doi.org/10.1016/j.smim.2016.03.004.

39. Sterlin, D., Mathian, A., Miyara, M., Mohr, A., Anna, F., Claër, L., Quentric, P., Fadlallah, J., Devilliers, H., Ghillani, P., et al. (2021). IgA dominates the early neutralizing antibody response to SARS-CoV-2. Sci. Transl. Med. 13, eabd2223. https://doi.org/10.1126/scitranslmed.abd2223.

40. Bartsch, Y.C., Wang, C., Zohar, T., Fischinger, S., Atyeo, C., Burke, J.S., Kang, J., Edlow, A.G., Fasano, A., Baden, L.R., et al. (2021). Humoral signatures of protective and pathological SARS-CoV-2 infection in children. Nat. Med. 27, 454–462. https://doi.org/10.1038/s41591-021-01263-3.

41. Hasan Ali, O., Bomze, D., Risch, L., Brugger, S.D., Paprotny, M., Weber, M., Thiel, S., Kern, L., Albrich, W.C., Kohler, P., et al. (2021). Severe coronavirus disease 2019 (COVID-19) is associated with elevated serum immunoglobulin (ig) A and antiphospholipid IgA antibodies. Clin. Infect. Dis. 73, e2869–e2874. https://doi.org/10.1093/cid/ciaa1496.

42. Gimpel, A.K., Maccataio, A., Unterweger, H., Sokolova, M.V., Schett, G., and Steffen, U. (2021). IgA complexes induce neutrophil extracellular

trap formation more potently than IgG complexes. Front. Immunol. 12, 761816. https://doi.org/10.3389/fimmu.2021.761816.

43. Aleyd, E., van Hout, M.W.M., Ganzevles, S.H., Hoeben, K.A., Everts, V., Bakema, J.E., and van Egmond, M. (2014). IgA enhances NETosis and release of neutrophil extracellular traps by polymorphonuclear cells via Fcα receptor I. J. Immunol. 192, 2374–2383. https://doi.org/10.4049/jimmunol.1300261.

44. Qi, H., Yang, S., and Zhang, L. (2017). Neutrophil extracellular traps and endothelial dysfunction in atherosclerosis and thrombosis. Front. Immunol. 8, 928. https://doi.org/10.3389/fimmu.2017.00928.

45. Denning, N.L., Aziz, M., Gurien, S.D., and Wang, P. (2019). DAMPs and NETs in sepsis. Front. Immunol. 10, 2536. https://doi.org/10.3389/fimmu.2019.02536.

46. de Bont, C.M., Boelens, W.C., and Pruijn, G.J.M. (2019). NETosis, complement, and coagulation: a triangular relationship. Cell. Mol. Immunol. 16, 19–27. https://doi.org/10.1038/s41423-018-0024-0.

47. Yonker, L.M., Boucau, J., Regan, J., Choudhary, M.C., Burns, M.D., Young, N., Farkas, E.J., Davis, J.P., Moschovis, P.P., Bernard Kinane, T., et al. (2021). Virologic features of severe acute respiratory syndrome coronavirus 2 infection in children. J. Infect. Dis. 224, 1821–1829. https://doi.org/10.1093/infdis/jiab509.

48. Bastard, P., Gervais, A., Le Voyer, T., Rosain, J., Philippot, Q., Manry, J., Michailidis, E., Hoffmann, H.H., Eto, S., Garcia-Prat, M., et al. (2021). Autoantibodies neutralizing type I IFNs are present in ~4% of uninfected individuals over 70 years old and account for ~20% of COVID-19 deaths. Sci. Immunol. 6, eabl4340. https://doi.org/10.1126/sciimmunol.abl4340.

49. Jacobs, J.L., Bain, W., Naqvi, A., Staines, B., Castanha, P.M.S., Yang, H., Boltz, V.F., Barratt-Boyes, S., Marques, E.T.A., Mitchell, S.L., et al. (2022). SARS-CoV-2 viremia is associated with COVID-19 severity and predicts clinical outcomes. Clin. Infect. Dis. 74, 1525–1533. https://doi.org/10.1093/cid/ciab686.

50. Li, Y., Schneider, A.M., Mehta, A., Sade-Feldman, M., Kays, K.R., Gentili, M., Charland, N.C., Gonye, A.L., Gushterova, I., Khanna, H.K., et al. (2021). SARS-CoV-2 viremia is associated with distinct proteomic pathways and predicts COVID-19 outcomes. J. Clin. Invest. 131, 148635. https://doi.org/10.1172/jci148635.

51. Yonker, L.M., Swank, Z., Gilboa, T., Senussi, Y., Kenyon, V., Papadakis, L., Boribong, B.P., Carroll, R.W., Walt, D.R., and Fasano, A. (2022). Zonulin antagonist, larazotide (AT1001), as an adjuvant treatment for multisystem inflammatory syndrome in children: a case series. Crit. Care Explor. 10, e0641. https://doi.org/10.1097/cce.0000000000000641.

52. Lima, R., Gootkind, E.F., De la Flor, D., Yockey, L.J., Bordt, E.A., D'Avino, P., Ning, S., Heath, K., Harding, K., Zois, J., et al. (2020). Establishment of a pediatric COVID-19 biorepository: unique considerations and opportunities for studying the impact of the COVID-19 pandemic on children. BMC Med. Res. Methodol. 20, 228. https://doi.org/10.1186/s12874-020-01110-y.

53. Villani, A.C., Satija, R., Reynolds, G., Sarkizova, S., Shekhar, K., Fletcher, J., Griesbeck, M., Butler, A., Zheng, S., Lazo, S., et al. (2017). Single-cell RNA-seq reveals new types of human blood dendritic cells, monocytes, and progenitors. Science 356, eaah4573. https://doi.org/10.1126/science.aah4573.

54. Edwards, A., and Haas, W. (2016). Multiplexed quantitative proteomics for high-throughput comprehensive proteome comparisons of human cell lines. Methods Mol. Biol. 1394, 1–13. https://doi.org/10.1007/978-1-4939-3341-9_1.

55. Hughes, C.S., Moggridge, S., Müller, T., Sorensen, P.H., Morin, G.B., and Krijgsveld, J. (2019). Single-pot, solid-phase-enhanced sample preparation for proteomics experiments. Nat. Protoc. 14, 68–85. https://doi.org/10.1038/s41596-018-0082-x.

56. Lapek, J.D., Jr., Greninger, P., Morris, R., Amzallag, A., Pruteanu-Malinici, I., Benes, C.H., and Haas, W. (2017). Detection of dysregulated protein-association networks by high-throughput proteomics predicts cancer

vulnerabilities. Nat. Biotechnol. *35*, 983–989. https://doi.org/10.1038/nbt.3955.

57. Li, J., Van Vranken, J.G., Pontano Vaites, L., Schweppe, D.K., Huttlin, E.L., Etienne, C., Nandhikonda, P., Viner, R., Robitaille, A.M., Thompson, A.H., et al. (2020). TMTpro reagents: a set of isobaric labeling mass tags enables simultaneous proteome-wide measurements across 16 samples. Nat. Methods *17*, 399–404. https://doi.org/10.1038/s41592-020-0781-4.

58. McAlister, G.C., Nusinow, D.P., Jedrychowski, M.P., Wühr, M., Huttlin, E.L., Erickson, B.K., Rad, R., Haas, W., and Gygi, S.P. (2014). MultiNotch MS3 enables accurate, sensitive, and multiplexed detection of differential expression across cancer cell line proteomes. Anal. Chem. *86*, 7150–7158. https://doi.org/10.1021/ac502040v.

59. Ting, L., Rad, R., Gygi, S.P., and Haas, W. (2011). MS3 eliminates ratio distortion in isobaric multiplexed quantitative proteomics. Nat. Methods *8*, 937–940. https://doi.org/10.1038/nmeth.1714.

60. Erickson, B.K., Jedrychowski, M.P., McAlister, G.C., Everley, R.A., Kunz, R., and Gygi, S.P. (2015). Evaluating multiplexed quantitative phospho-peptide analysis on a hybrid quadrupole mass filter/linear ion trap/orbitrap mass spectrometer. Anal. Chem. *87*, 1241–1249. https://doi.org/10.1021/ac503934f.

61. Erickson, B.K., Mintseris, J., Schweppe, D.K., Navarrete-Perea, J., Erickson, A.R., Nusinow, D.P., Paulo, J.A., and Gygi, S.P. (2019). Active instrument engagement combined with a real-time database search for improved performance of sample multiplexing workflows. J. Proteome Res. *18*, 1299–1306. https://doi.org/10.1021/acs.jproteome.8b00899.

62. Eng, J.K., McCormack, A.L., and Yates, J.R. (1994). An approach to correlate tandem mass spectral data of peptides with amino acid sequences in a protein database. J. Am. Soc. Mass Spectrom. *5*, 976–989. https://doi.org/10.1016/1044-0305(94)80016-2.

63. Huttlin, E.L., Jedrychowski, M.P., Elias, J.E., Goswami, T., Rad, R., Beausoleil, S.A., Villén, J., Haas, W., Sowa, M.E., and Gygi, S.P. (2010). A tissue-specific atlas of mouse protein phosphorylation and expression. Cell *143*, 1174–1189. https://doi.org/10.1016/j.cell.2010.12.001.

64. Elias, J.E., and Gygi, S.P. (2007). Target-decoy search strategy for increased confidence in large-scale protein identifications by mass spectrometry. Nat. Methods *4*, 207–214. https://doi.org/10.1038/nmeth1019.

65. Graubert, A., Aguet, F., Ravi, A., Ardlie, K.G., and Getz, G. (2021). RNA-SeQC 2: efficient RNA-seq quality control and quantification for large cohorts. Bioinformatics *37*, 3048–3050. https://doi.org/10.1093/bioinformatics/btab135.

66. Love, M.I., Huber, W., and Anders, S. (2014). Moderated estimation of fold change and dispersion for RNA-seq data with DESeq2. Genome Biol. *15*, 550. https://doi.org/10.1186/s13059-014-0550-8.

67. Puram, S.V., Tirosh, I., Parikh, A.S., Patel, A.P., Yizhak, K., Gillespie, S., Rodman, C., Luo, C.L., Mroz, E.A., Emerick, K.S., et al. (2017). Single-cell transcriptomic analysis of primary and metastatic tumor ecosystems in head and neck cancer. Cell *171*, 1611–1624.e24, e1624. https://doi.org/10.1016/j.cell.2017.10.044.

68. Schindelin, J., Arganda-Carreras, I., Frise, E., Kaynig, V., Longair, M., Pietzsch, T., Preibisch, S., Rueden, C., Saalfeld, S., Schmid, B., et al. (2012). Fiji: an open-source platform for biological-image analysis. Nat. Methods *9*, 676–682. https://doi.org/10.1038/nmeth.2019.

69. Tinevez, J.Y., Perry, N., Schindelin, J., Hoopes, G.M., Reynolds, G.D., Laplantine, E., Bednarek, S.Y., Shorte, S.L., and Eliceiri, K.W. (2017). TrackMate: an open and extensible platform for single-particle tracking. Methods *115*, 80–90. https://doi.org/10.1016/j.ymeth.2016.09.016.

STAR★METHODS

KEY RESOURCES TABLE

REAGENT or RESOURCE	SOURCE	IDENTIFIER
Antibodies		
FITC anti-human CD66b	BioLegend	CAT# 305103; RRID:AB_314495
Pacific Blue™ anti-human CD14 Antibody	BioLegend	CAT# 325615; RRID:AB_830688
Biological samples		
Patient samples used in this study are described in Tables 1, S3, and S4	Massachusetts General Hospital	N/A
Chemicals, peptides, and recombinant proteins		
DRAQ5®	Cell Signaling Technology	CAT #4084
SYTOX™ Green Nucleic Acid Stain	Invitrogen	CAT# S7020
Phorbol 12-myristate 13-acetate	Sigma Aldrich	CAT# P1585
Ficoll® Paque Plus	Cytiva	CAT# 17-1440-03
Buffer TCL	Qiagen	CAT# 1031576
β-mercaptoethanol	Sigma Aldrich	CAT# M6250
Hoechst 33,342 Solution	Thermo Fisher Scientific	CAT# 62249
Critical commercial assays		
EasySep™ Direct Human Neutrophil Isolation Kit	STEMCELL Technologies	CAT# 19666
HetaSep™	STEMCELL Technologies	CAT# 07806
Qubit dSDNA High Sensitivity Assay Kit	Invitrogen	CAT #Q32854
High-Sensitivity DNA Bioanalyzer Kit	Agilent	CAT# 5067-4626
Nextera XT Library Prep kit	Illumina	CAT# FC-131-1024
Deposited data		
Neutrophil bulk RNAseq analyzed data	This manuscript	GEO: GSE217370 https://www.ncbi.nlm.nih.gov/geo/query/acc.cgi?acc=GSE217370
Adult COVID-19 Neutrophil bulk RNA-seq data	LaSalle et al. 2022	GEO: GSE212041
COVID-19 Neutrophil scRNA-Seq data	Schulte-Schrepping et al. 2020	EGA accession -EGAS00001004571
Sepsis Neutrophil scRNA-seq data	Reyes et al. 2021	https://singlecell.broadinstitute.org/single_cell/study/SCP1492/
ARDS Neutrophil RNA-Seq	Juss et al. 2016	GEO accession GSE76293
Lung cancer single-cell neutrophil RNA-seq data	Zilionis et al. 2019	GEO: GSE127465
Oligonucleotides		
RT primer (DNA oligo)	IDT	5′-AAGCAGTGGTATCAACGCAGAGTACT30VN-3′
TSO primer (RNA oligo with LNA)	Qiagen	5-AAGCAGTGGT ATCAACGCAGAG TACATrGrG + G-3′
ISPCR (DNA oligo)	IDT	5′-AAGCAGTGGT ATCAACGCAGAG T-3′
Software and algorithms		
Code and Data from this manuscript	This manuscript	https://doi.org/10.5281/zenodo.7277479 https://doi.org/10.5281/zenodo.7277353
FIJI Is Just ImageJ	NIH	https://imagej.net/software/fiji/
IntelliCyt ForeCyt (v8.1)	Sartorius	https://www.sartorius.com/en/products/flow-cytometry/flow-cytometry-software
INSPIRE software	EMD Millipore	https://www.emdmillipore.com/US/en/20150212_143429
IDEAS software	EMD Millipore	https://www.emdmillipore.com/US/en/20150212_144049
AutoCAD	Autodesk	https://www.autodesk.com/products/autocad/overview

(Continued on next page)

Continued

REAGENT or RESOURCE	SOURCE	IDENTIFIER
GTEx-TOPMed RNA-Seq pipeline	Broad Institute	https://github.com/broadinstitute/gtexpipeline/
STAR v2.5.3a	Dobin et al., 2013	https://github.com/alexdobin/STAR/releases/tag/2.5.3a
RSEM v1.3.0	Li et al., 2011	https://github.com/deweylab/RSEM/releases/tag/v1.3.0
RNA-SeQC 2	Graubert et al. 2021	https://github.com/getzlab/rnaseqc
CIBERSORTx	Newman et al., 2019	https://cibersortx.stanford.edu
DESeq2 v1.30.1	Love et al., 2014	https://bioconductor.org/packages/release/bioc/html/DESeq2.html
Fgsea	Korotkevich et al., 2019	http://bioconductor.org/packages/release/bioc/html/fgsea.html
Prism 9.3.1 (471)	GraphPad	https://www.graphpad.com/scientific-software/prism/
sigPathway v1.64.0	Lai et al., 2022	https://bioconductor.org/packages/release/bioc/html/sigPathway.html
Other		
FluoSpheres™ NeutrAvidin™-Labeled Microspheres, 1.0 μm, yellow-green fluorescent (505/515), 1% solids	Invitrogen	CAT #F8776
CaptureSelect™ IgA Affinity Matrix	Thermo Fisher Scientific	CAT #194288010
Protein G Resin	GenScript	CAT #L00209

RESOURCE AVAILABILITY

Lead contact
Further information and requests for resources and reagents should be directed to and will be fulfilled by the lead contact, Lael Yonker (lyonker@mgh.harvard.edu).

Materials availability
This study did not generate new unique reagents.

Data and code availability
- Due to IRB consent limitations, raw sequencing data is not publicly available. However, the read count matrix and TPM matrix used in this study will be publicly available in GEO (Gene Expression Omnibus) under accession number GSE217370 (https://www.ncbi.nlm.nih.gov/geo/query/acc.cgi?acc=GSE217370) and Table S5. Additional Supplemental Items are available from Zenodo Data: https://doi.org/10.5281/zenodo.7277479. Raw sequencing data can be made available from the lead contact upon request.
- All code required to run the analyses in this manuscript is deposited in Zenodo Data: https://doi.org/10.5281/zenodo.7277479 based on the associated Github repository (https://github.com/lasalletj/Pediatric_COVID_MISC_Neutrophils).
- Any additional information required to reanalyze the data reported in this work paper is available from the lead contact upon request.

EXPERIMENTAL MODEL AND SUBJECT DETAILS

MGH patient cohort description
Biospecimens were obtained from pediatric patients at Massachusetts General Hospital (MGH) under the institutional review board (IRB) approved 'MGH Pediatric COVID-19 Biorepository' (no. 2020P000955). Healthy pediatric controls were collected under the IRB-approved 'the Center for Celiac Research Pediatric Biorepository' (no. 2016P000949). Informed consent, and assent, when appropriate, were obtained in accordance with IRB guidelines from patients and/or parents/guardians before study enrollment. Patients classified as COVID-19 positive had positive SARS-CoV-2 RT-PCR results upon enrollment. Patients classified as MIS-C were diagnosed per CDC guidelines. Healthy children were children presenting for well-child visits, a vaccine appointment, or an endoscopy (with normal pathology), and are otherwise healthy. Non-COVID-19 pediatric controls were children that were sick (hospitalized or outpatient) during the pandemic but tested negative for SARS-CoV-2.

METHOD DETAILS

Neutrophil isolation and lysis

Blood samples were processed as previously described.[1,52] Briefly, blood samples were collected in vacutainer tubes containing EDTA anticoagulant. Whole blood was centrifuged at room temperature at 1000g for 10 min with breaks activated to allow for plasma collection. The remaining blood was mixed 1:1 with HBSS and gently layered on top of Ficoll at a 2:1 ratio. This was centrifuged at room temperature at 1000g for 30 min with the brakes off. PBMCs were then removed, and neutrophils were isolated from the remaining blood pellet via negative selection using the EasySep Direct Neutrophil Isolation Kit (STEMCELL Technologies, Cat# 19666), following manufacturer's directions. 1×10^5 cells were centrifuged at 300g for 5 min at room temperature with soft brakes activated. Neutrophils were lysed with 100 μL of RNA lysis buffer (TCL) (Qiagen, Cat# 1031576) with 1% β-mercaptoethanol and frozen at −80°C.

Validation of isolated neutrophil purity

Nucleated cells were collected from whole blood via red blood cell sedimentation using HetaSep solution (STEMCELL Technologies, Cat# 07906). Neutrophils were isolated as previously described (plasma centrifuged, PBMCs isolated and collected, and neutrophils isolated from remaining red blood cell pellet). Isolated neutrophils and nucleated cells were centrifuged at 300g for 5 min at room temperature with the brakes off. The cells were resuspended in 50 μL of FACS buffer (0.5% BSA in PBS) and then fixed in 1% paraformaldehyde in PBS. All fixed cells were then stained with CD66b (1:200 dilution) (Biolegend, Cat# 305103), CD14 (1:20 dilution) (Biolegend, Cat# 325615), and DRAQ5 (1:2000 dilution) (Cell Signaling Technology, Cat# 4084S). Data was obtained through the Amnis ImageStreamX Mark II imaging flow cytometer and INSPIRE software (EMD Millipore). The accompanying IDEAS software (EMD Millipore) was used to perform data analysis. Additionally, Giemsa staining was performed on the isolated neutrophils to ensure no contamination of eosinophils. The isolated neutrophil solution was prepared in PBS at a concentration of 1×10^5 cells/mL. Cytospin preparations were made at 600 RPM for 5 min, and the cells allowed to air dry overnight. The next morning, cells were stained with fixative, eosin, and methylene blue (Thermo Fisher Scientific, Cat# 9990701), washed with DI water, and left to dry overnight. The cells and slide were mounted in the morning. Images were captured using a ZEISS Stemi 305 stereo microscope.

Patient matched plasma isolation

Blood samples were processed as previously described.[52] Briefly, blood samples were collected in EDTA vacutainer tubes. Plasma was collected by centrifuging tubes at 1000g for 10 min at room temperature with brakes activated. Aliquoted plasma was stored at −80°C.

Smart-Seq2 cDNA preparation

cDNA was prepared from bulk populations of 1×10^5 neutrophils as recently described[1] using a modified reverse transcription step.[53] Neutrophil lysates were thawed on ice, and 20 μL per sample was added to a 96-well plate prior to brief centrifugation. Following RNA purification with Agencourt RNAClean XP SPRI beads (Beckman Coulter, Cat# A63987), samples were resuspended in 4 μL of Mix-1 [Per 1 sample: 1 μL (10 μM) RT primer (DNA oligo) 5′–AAGCAGTGGTATCAACGCAGAGTACT30VN-3′; 1 μL (10 μM) dNTPs; 1μL (10%, 4 U/μL) recombinant RNase inhibitor; 1 μL nuclease-free water], denatured at 72°C for 3 min and immediately cooled on ice for 1 min. Next, 7 μL of Mix-2 [Per 1 sample: 0.75 μL nuclease-free water; 2 μL 5X RT buffer (Thermo Fisher Scientific, Cat# EP0753); 2 μL (5 M) betaine; 0.9 μL (100 mM) MgCl2; 1 μL (10 μM) TSO primer (RNA oligo with LNA) 5′-AAGCAGTGGTATCAACGCAGAGTACATrGrG + G-3′; 0.25 μL (40 U/μL) recombinant RNase inhibitor; 0.1 μL (200 U/μL) Maxima H Minus Reverse Transcriptase] was added. Reverse transcription was performed at 50°C for 90 min, followed by a 5-min incubation at 85°C. Next, 14 μL of Mix-3 [Per 1 sample: 1 μL nuclease-free water; 0.5 μL (10 μM) ISPCR primer (DNA oligo) 5′-AAGCAGTGGTATCAACGCAGAGT-3′; 12.5 μL 2X KAPA HiFi HotStart ReadyMix] was added to each well and amplification was performed at 98°C for 3 min, followed by 16 cycles of [98°C for 15 s, 67°C for 20 s, and 72°C for 6 min], and final extension at 72°C for 5 min. Primer removal and cDNA purification was performed using AgencourtAMPureXP SPRI beads (Beckman Coulter, Cat# A63881). Concentration measurements were determined with the Qubit dsDNA high sensitivity assay kit (Invitrogen, Cat# Q32854) on the Cytation 5 Microplate Reader (BioTek), and cDNA size distribution was measured using the High-Sensitivity DNA Bioanalyzer Kit (Agilent, Cat# 5067-4626).

Library construction and sequencing

Libraries were constructed with the Nextera XT Library Prep kit (Illumina, Cat# FC-131-1024) using custom indexing adapters[53] in a 384-well PCR plate. Residual primer dimers were removed with an additional cleanup step. One pooled library containing 26 samples were sequenced on a NextSeq 500 sequencer (Illumina) using paired-end 38-base reads. Following quality control and acquisition of additional samples, a second pooled library containing 40 samples was sequenced using the same method.

Spontaneous NET release fluorescence microscopy data acquisition

Blood was processed from healthy pediatric and MIS-C patients as previously described.[52] An aliquot of 1×10^4 cells in 50 μL RPMI (no FBS) was collected from the isolated neutrophils. Neutrophils were plated in a single well of a black, clear-bottom 96-well plate. 50 μL of RPMI was added to the well for the unstimulated neutrophils. For the stimulated neutrophils, 50 μL of phorbol myristate

acetate (PMA) (Sigma Aldrich, Cat# P1585) was added to a final concentration of 100 nM. 50 μL of SYTOX green (Thermo Fisher Scientific, Cat# S7020) in RPMI was added to a final concentration of 2 μM. NETosis was imaged using the Personal AUtomated Lab Assistant (PAULA) Cell Imager (Leica Microsystems) placed in a 37°C incubator with 5% CO_2. Brightfield and FITC images were taken every 10 min for 4 h to allow for temporal imaging of NET formation.

Cell-free DNA quantification

cfDNA quantification was performed using the Qubit dsDNA High Sensitivity Assay Kit (Invitrogen, Cat# Q32854) according to the manufacturer's protocol. 98 μL of Qubit DNA dye was aliquoted per well of a 96-well black clear bottom plate (Corning, Cat# 3904). 2 μL of plasma sample was added to each well of the assay plate, and fluorescence was measured on a Cytation 5 Microplate reader at 523 nm. The concentration of cell-free DNA was analyzed relative to the average concentration of the healthy controls.

Plasma protein measurement

Samples were prepared as previously described.[6] 100 μg were denatured, reduced, alkylated, and purified using solid-phase-enhanced sample-preparation (SP3) technology before lysc and tryptic digest.[54,55] 25 μg of the resulting peptides were subsequently labeled using TMTpro reagents (Thermo Fisher Scientific) according to the manufacturer's instructions.[56,57] Labeled samples were combined and fractionated using a basic reversed phase HPLC.[54] The fractions were analyzed via reversed phase LC-M2/MS3 on either an Orbitrap Fusion Lumos or an Orbitrap Eclipse mass spectrometer using the Simultaneous Precursor Selection (SPS) supported MS3 method[58,59] essentially as described previously[60] and using Real-Time Search when using the Orbitrap Eclipse.[61] MS2 spectra were assigned using a SEQUEST-based[62] in-house built proteomics analysis platform[63] using a target-decoy database-based search strategy to assist filtering for a false-discovery rate (FDR) of protein identifications of less than 10%.[64] Searches were done using the Uniprot human protein sequence database (UP000005640)[64] using an in-house-built platform.[62] Search strategy included a target-decoy database-based search in order to filter against a false-discovery rate (FDR) of protein identifications of less than 1%.[64] An average signal-to-noise value of larger than 10 per reporter ion as well as with an isolation specificity[59] of larger than 0.75 were considered for quantification. Lysozyme, Myeloperoxidase, collagenase matrix metallopeptidase 9, Lactoferrin, and Cathelicidin antimicrobial peptide were quantified. Protein concentration data were normalized as previously described.[56]

Design and fabrication of the microfluidic devices

Microfluidic devices used for time-lapse imaging of NETosis were designed using AutoCAD (Autodesk) and fabricated using standard photolithographic and soft lithography approaches (Figures S5A and S5B). Briefly, a master negative mold was prepared by spin-coating a silicon wafer with negative photoresist (SU-8, Microchem) to a thickness of 100 μm. The design was patterned onto the wafer by exposure to UV light through a mylar mask (Fineline Imaging) and developing away the unexposed areas. The silicon wafer was then used as a template for casting PDMS devices. PDMS base and primer were mixed at a ratio of 10:1 and poured over the wafer, degassed for at least 1 h, then baked overnight at 65°C. Inlets and outlets were punched using a 1 mm diameter biopsy punch (Harris UniCore, Millipore Sigma), and the entire device was liberated from the PDMS block using an 8 mm diameter punch. PDMS devices were treated with oxygen plasma and bonded irreversibly to oxygen plasma-treated glass-bottom well plates (Mattek) by heating to 75°C for 10 min.

Immune complex generation

Immune complexes were generated as previously described.[40] Briefly, SARS-CoV-2 Spike proteins were biotinylated, conjugated to NeutrAvidin beads, and incubated with 1:10 diluted plasma samples.

Plasma IgG and IgA depletion

IgG and IgA were depleted from MIS-C plasma samples as previously described.[40] Briefly, IgG was depleted using Protein A/G Agarose (Fisher Scientific, Cat# NC1466772) and IgA using CaptureSelect IgA Affinity Matrix (Thermo Fisher Scientific, Cat# 194288010). Pierce Centrifuge Columns were washed with 1X PBS and incubated overnight with the plasma samples. Depleted plasma was collected the following day by centrifugation of the columns. Control of a non-depleted plasma sample was treated identically but without adding the affinity matrix.

NETosis assay

10 μL of RPMI was loaded into the inlet port of the microfluidic device until a droplet was formed on the outlet port. RPMI was added to the wells until the devices were submerged. The plate was placed in a 37°C, 5% CO_2 incubator until the neutrophil solution was prepared to be loaded. Neutrophils were isolated from a healthy patient cohort. 1–2 mL of whole blood was collected in EDTA vacutainer tubes, and neutrophils were isolated via negative selection using the Easysep Direct Neutrophil Isolation Kit, following the manufacturer's directions. Isolated neutrophils were stained with 32 μM Hoechst 3342 dye for 10 min at 37°C, with 5% CO_2. Stained neutrophils were resuspended in RPMI (no FBS) to a concentration of 1×10^7 cells/mL. 10 μL of cells were mixed with 10 μL of stimulant and 10 μL of SYTOX green in RPMI (no FBS) to a final concentration of 2 μM. 5 μL of this solution was loaded into the inlet port of the microfluidic device using a standard pipette tip until cells were observed to exit the outlet port. Brightfield and FITC fields were imaged at 10x magnification using a fully automated fluorescent Nikon TiE inverted wide-field microscope

with a bio chamber heated to 37°C with 5% CO2. Each device was imaged every 12 min for 4 h to allow for temporal imaging of NET formation (Figure S5C). An initial image was taken with brightfield and DAPI at the beginning of the experiment to count fluorescently stained neutrophils.

QUANTIFICATION AND STATISTICAL ANALYSIS

RNA-seq alignment
Raw FASTQ files were aligned to a custom genome using the Terra platform of the Broad Institute. Alignment was performed using STAR v2.5.3a, and expression quantification was performed using RSEM v1.3.0. The custom FASTA was generated from the *Homo sapiens* genome assembly GRCh38 (hg38, excluding ALT, HLA, and Decoy contigs according to the Broad Institute GTEx-TOPMed RNA-seq pipeline, https://github.com/broadinstitute/gtex-pipeline/) with an appended SARS-CoV-2 genome. GENCODE v35 with the appended SARS-CoV2 GTF was used for annotation.

Quality control
RNA-SeQC 2[65] (https://github.com/getzlab/rnaseqc) was used to calculate quality control metrics for each sample. Samples were excluded if they did not meet the following criteria: 1) percentage of mitochondrial reads less than 20%, 2) greater than 10,000 genes detected with at least 5 unambiguous reads, 3) median exon CV less than 1, 4) exon CV MAD less than 0.75, 5) exonic rate greater than 25%, 6) median 3′ bias less than 90%. One sample was excluded for having low neutrophil content and high B cell contamination as estimated by CIBERSORTx, described in the next section. Only one sample was kept per patient: if more than one passed quality control, the earlier or pre-treatment sample was selected. Thus, out of 55 sequencing reactions, 48 samples were carried forward for analysis. Genes were included in the analysis if they were expressed at a level of 0.1 TPM in at least 20% of samples and if there were at least 6 counts in 20% of samples. In total, 15,406 genes passed the filtration criteria.

Neutrophil fraction estimation and contamination control
CIBERSORTx[16] was used to estimate total neutrophil, mature neutrophil, immature neutrophil, T/NK cells (either T or NK, due to similar gene expression profiles), B, plasmablast, and monocyte content in each sample. We generated a signature matrix from the single-cell RNA-seq data of PBMCs and neutrophils from whole blood from Cohort 2 of the Schulte-Schrepping et al. dataset (2)[4] using the pseudobulking method previously described.[1] CIBERSORTx was run using default parameters.

Dimensionality reduction and visualization
PCA and UMAP were performed in R using prcomp() and umap() with default parameters.

Differential expression analysis
Differential expression analyses were performed using the DESeq2 package in R[66] without additional covariates.

Gene set enrichment analysis and sigPathway
Gene set enrichment analysis was performed using the fgsea package in R using MSigDB Release v7.2 pathways from the H, C5 GO BP databases. We also added custom MSigDB pathways using the keyword "neutrophil," and the gmt file is available on Zenodo. In addition, we added gene sets defining neutrophil states in ARDS,[10] blood and lung tissue of lung cancer patients,[18] sepsis (20), single-cell neutrophil clusters in COVID-19 [4], and bulk RNA-seq signatures of neutrophils in COVID-19 [1]. sigPathway was performed using the sigPathway v1.64.0 package in R using the custom neutrophil state gene sets described above with all other parameters set to default.

Sample pathway scoring
Bulk RNA-seq samples were scored according to their expression of NMF neutrophil state gene signatures according to a previously described method used to control for sample complexity.[67] We defined the pathway score for each sample as the average expression of the genes in the gene set minus the average expression of genes in a control gene set. Genes were ranked according to average expression across all samples and divided into 25 bins, and for each gene in the NMF signature, 100 different genes were selected from the same bin to create a control gene set with comparable expression levels which is 100-fold larger.

Disease marker gene selection and heatmap
To identify genes uniquely associated with acute pediatric COVID-19 or MIS-C, we performed three differential expression analyses: MIS-C vs. COVID-19 and controls, COVID-19 vs. MIS-C and controls, and controls vs. MIS-C and COVID-19. We filtered the results for padj >0.05 and only selected positive markers (log(fold-change) greater than 0) and capped the lists at 50 genes. There were no significant marker genes for control neutrophils. Heatmaps of the gene markers for the two diseases were generated with the pheatmap package in R. Row (genes) are ordered according to p value, and columns are ordered according to the clinical subtypes shown in the legend.

CellPress
OPEN ACCESS

Quantification of NETosis

Detection of NETs was performed automatically on the FITC channel using the TrackMate plugin in FIJI.[68,69] As neutrophils undergo NETosis, the nucleus undergoes condensation, followed by decondensation of the chromatin. Next, the cell's nuclear membrane breaks down, allowing for SYTOX green to stain the DNA and (Figure S5D). NETs are quickly dispersed, and the fluorescence is diffused (Figure S5E). Non-NETosis cellular death can become stained with SYTOX green as the membrane breaks down, however, the fluorescence signal is stable and long-lasting (Figure S5F). The methodology was validated using manual tracking within FIJI[68] to determine the average length of time of cells undergoing NETosis against cells undergoing non-NETosis cellular death. A cutoff differentiating the two was defined at 1.5 h (Figure S4G). Thus, NETs were defined as tracked cells with a duration ≤ 1.5 h, and non-NETosis cellular death was defined as tracked cells with a course> 1.5 h (Movie S3). A total number of neutrophils was counted using the DAPI channel at time t = 0 [68]. The percentage of NETs was calculated using the number of NETs released at a specific time point divided by the total number of neutrophils.

Statistical analysis

To compare multiple groups, results were compared by 1-way ANOVA with multiple comparisons or by Kruskal-Wallis with post-hoc comparisons between the groups completed using Dunn's test and corrected for multiple comparisons with Tukey's method in GraphPad Prism v9. Statistical tests used are noted in the figure caption. Statistical significance is defined as $*p < 0.05$, $**p < 0.01$, $***p < 0.001$, and $****p < 0.0001$, unless otherwise noted in the figure.